Electrochimica Acta 366 (2021) 137431

Contents lists available at ScienceDirect

Electrochimica Acta

journal homepage: www.elsevier.com/locate/electacta

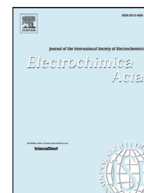

The effect of surface preparation on the protective properties of Al_2O_3 and HfO_2 thin films deposited on cp-titanium by atomic layer deposition

Ivan Spajić [a,b], Peter Rodič [a], Gavrilo Šekularac [a], Maria Lekka [c], Lorenzo Fedrizzi [c], Ingrid Milošev [a,*]

[a] Jožef Stefan Institute, Department of Physical and Organic Chemistry, Jamova c. 39, Ljubljana, SI-1000, Slovenia
[b] Jožef Stefan International Postgraduate School, Jamova c. 39, SI-1000 Ljubljana, Slovenia
[c] University of Udine, Polytechnic Department of Engineering and Architecture, Via delle Scienze 206, Udine, 33100, Italy

ARTICLE INFO

Article history:
Received 1 August 2020
Revised 2 November 2020
Accepted 3 November 2020
Available online 5 November 2020

Keywords:
Atomic layer deposition
Alumina
Hafnia
Cp-titanium
Chemical-mechanical polishing

ABSTRACT

Atomic layer deposition (ALD), a method that allows the formation of thin and conformal films on substrates of interest, was employed to prepare thin films of alumina (Al_2O_3) and hafnia (HfO_2), with the aim of protecting the surface of the commercially pure titanium (cp-Ti) used in biomedical applications. Prior to deposition, cp-Ti specimens have been prepared in two ways – grinding and grinding followed by polishing. Such surfaces have been denoted as rough and smooth, respectively. The thickness, composition, morphology and topography of alumina and hafnia films have been determined using ellipsometry, focused ion beam microscopy with energy dispersive X-ray spectroscopy, time-of-flight secondary ion mass spectrometry and 3D profilometry. A homogeneous stoichiometric composition of alumina and hafnia was obtained with a layer thickness of ca. 150 nm. The anti-corrosive properties of ALD thin films were measured in simulated body fluid solution, using electrochemical impedance spectroscopy (EIS) and potentiodynamic polarization curves. The roughness of the cp-Ti surface plays an important role in the protective properties of these films, especially those of hafnia. In general, when deposited on a smooth surface, ALD films with better anti-corrosive properties were obtained, as evidenced by EIS long-term, 40-day tests. ALD films showed very low porosity, calculated from electrochemical parameters, and significantly lower corrosion current densities, compared with those from bare cp-Ti specimens. Lower porosity and slightly better protective properties were provided by films of hafnia. On the other hand, according to EIS long-term tests, alumina retained slightly greater impedance values than hafnia. Since both alumina and hafnia are biocompatible materials, this study confirms the possibility of their use to reduce the risk of failure of medical implants made of cp-Ti, in the human body environment.

© 2020 The Authors. Published by Elsevier Ltd.
This is an open access article under the CC BY-NC-ND license
(http://creativecommons.org/licenses/by-nc-nd/4.0/)

1. Introduction

Stainless steel, Co–Cr- and Ti-based alloys are the most common metallic biomaterials used for biomedical purposes, e.g., implant devices [1,2]. The main advantage of Ti and its alloys is their highest corrosion resistance, thanks to the highly stable passive film of TiO_2 that forms spontaneously in the presence of oxygen on the Ti surface [3]. Another feature necessary for biomaterials is biocompatibility, and Ti-based alloys have proved to be the most desirable by this criterion [2,4]. Biocompatibility is also related to osseointegration, the ability of human bone cells to bond and grow quite effectively on the surface of implant materials. The high ability to be osseointegrated is a specific characteristic of the Ti-based alloys typically used in biomedical applications, such as Ti–6Al–4V and Ti–6Al–7Nb and, in particular, of pure titanium. Again, this is due to the protective passive film of TiO_2, more precisely the hydrated Ti peroxy matrix that constitutes an interface between a Ti implant and living tissue [5–7]. Further, in order to be biocompatible, the mechanical properties, e.g., the Young's modulus, of the metallic biomaterial, should be as close as possible to those of the bone in order to avoid stress shielding [8]. Unfortunately, all metallic biomaterials display the latter disadvantage, as they generally have too high a Young's modulus. However, Ti-based alloys

* Corresponding author.
E-mail address: ingrid.milosev@ijs.si (I. Milošev).

https://doi.org/10.1016/j.electacta.2020.137431
0013-4686/© 2020 The Authors. Published by Elsevier Ltd. This is an open access article under the CC BY-NC-ND license (http://creativecommons.org/licenses/by-nc-nd/4.0/)

feature a lower Young's modulus, closer to that of bone than that of stainless steel and of Co–Cr-based alloys [2,5]. The critical point of Ti-based alloys and, especially, of pure Ti, is their susceptibility to wear due to friction or abrasive action when in contact with other materials in an implant device [4,5]. This is also the reason for the development of many Ti-based alloys, mainly for the purpose of improving wear resistance and for reducing the Young's modulus [2,9].

Technical Standard ASTM F67 [10] classifies commercially pure titanium (cp-Ti) for medical applications into four grades, G1 to G4, that differ in the proportion of trace elements (O, Fe, C, N and H). The interstitial solutes, O and N, play a major role because they tune the mechanical properties of cp-Ti [11]. Due to its limitations in mechanical properties, cp-Ti is used only where direct wear contact is minimal, mainly in dental surgery, as non-load bearing parts for some joints like the acetabular shell of the hip, for bone fixation materials like nails, screws, nuts and plates, housing devices for pacemakers, artificial heart valves etc. [5]. Although it has excellent anticorrosive properties, cp-Ti sometimes fails under the human body conditions. Bhola et al. in a comprehensive review [12] reported many *in-vitro* and *in-vivo* studies and cases that pointed out the problem of galvanic coupling of cp-Ti in contact with other metallic biomaterials that resulted in release of Ti ions in the periprosthetic tissue. In addition, galvanic coupling or cathodic charging may cause hydrogen to be evolved on Ti surfaces, which may then penetrate and cause hydrogen induced cracking in the titanium structure [12,13]. Fretting corrosion of titanium, related to its poor wear resistance, has often been reported to lead to the release of titanium debris particles [14–18]. But if the problem of corrosion or release of Ti ions is considered exclusively, the atomic layer deposition (ALD) technique, which has hitherto been seldom investigated, becomes an interesting solution to the protection against corrosion of biomedical materials [19].

The ALD technique allows the formation of nanoscale coatings, commonly referred to as thin films. Originally, it was known as Molecular Layering; it was invented in Russia by Aleskovski and co-workers in the 1960s [20]. The technique was then developed further by Suntola and Antson in Finland in the 1970s under the name of Atomic Layer Epitaxy, and was patented as a new technique for the growth of polycrystalline dielectric thin films with unique characteristics [21]. Initially, this technique was reserved exclusively for producing thin layers for *thin film electroluminescent displays*. Later, research advances have expanded the use of ALD technology from microelectronic applications (high-κ dielectrics in MOSFETs and DRAMs) to various protective coatings, optical applications and photocatalysis [22]. The first article that considered application of ALD thin films in corrosion protection was published in 1999 [23]. The first proposal on the use of ALD thin films for biomedical implants appeared in a patent from Argonne National Laboratory in 2006 [24]. Due to the great interest in ALD technology, a variety of materials and deposition processes have been developed in different fields of technology. However, up to now, studies on ALD thin films as protective coatings on biomedical implants have been focused mainly on only a few ceramic materials, such as alumina (Al_2O_3) [25,26] and zirconia (ZrO_2) [27] as bioinert materials, and as titania (TiO_2) [28] and hydroxyapatite (HA) [29] as bioactive materials. Despite the very high conformity and uniformity of the ALD films in general [30–32], they have some drawbacks that need to be investigated further to establish their application as biomedical implants. For example, alumina tends to grow as an amorphous film that provides good barrier properties but can be chemically unstable and, even, soluble in corrosive environments [23,32,33]. On the other hand, titania tends to grow as a polycrystalline film at temperatures above 150 °C and, although this makes it chemically stable in a corrosive environment, its grain boundaries constitute weak points at which penetration of corrosive electrolyte to the substrate can take place [23,33]. For this reason, the possibility of combining amorphous and polycrystalline alumina and titania films to produce multilayer films with the desired corrosion protection has been investigated [25,34,35]. Hafnia (HfO_2) and zirconia ALD thin films have been widely investigated for dielectric applications as high-κ materials [36]. However, although they have the potential to be applied as protective thin films on metallic biomaterials, they have, hitherto, been seldom investigated for biomedical purposes [37]. For this reason, the protective properties of alumina and hafnia ALD thin films deposited on cp-Ti as a substrate have been compared in this study.

The main aims were to investigate the electrochemical and microstructural properties of hafnia thin films prepared by ALD and, then, to compare them with those of alumina ALD thin film. Hafnia, as a thin film obtained by electrochemical anodization, has been reported to exhibit good biocompatibility and other properties required for biomedical applications [38]. Moreover, hafnium, as a pure metal that is spontaneously passivated with hafnia, has been investigated as an alternative for potential biomedical applications. It has shown very good biocompatibility as well as osteogenesis [39], but the main reason why hafnia thin film is interesting for further research is that it is chemically stable, being highly resistant to corrosive species [37], and that, unlike titania ALD thin film, provides the possibility of forming an amorphous film [40] of very low porosity and good barrier properties [37]. In addition, the crystallinity of the amorphous hafnia thin film increases slightly, up to ca. 10%, as the deposition temperature increases from 100 to 200 °C while, above 200 °C, it increases rapidly [40]. This increase may vary, depending on the precursors used, the process pressure and the substrate. In any case, this property of the hafnia ALD thin film can be used to easily control the crystallinity and, consequently, chemical stability and the barrier properties of the film. ALD thin films have been characterized by various techniques to elaborate their thickness, uniformity, morphology and topography i.e. ellipsometry, scanning electron microscopy with energy dispersive X-ray spectroscopy (SEM/EDXS), focused ion beam (FIB) microscopy with EDXS, time-of-flight secondary ion mass spectrometry (ToF-SIMS) and 3D profilometry.

Special emphasis has been given to the role of substrate surface roughness in the anti-corrosive or barrier properties of alumina and hafnia thin films. Surface roughness is very important for biomedical implant materials and can be a decisive factor in osseointegration and also bacteria colonization [41]. Thus, micro-roughness of the implant surface has been proved to promote interaction of an implant with bone or tissue [42], while the high degree of smoothness can be desirable, since it allows low friction and good sliding in the contact between the implant components, such as in the joint [43].

2. Experimental details

2.1. Metal substrates and chemicals

As substrate material, commercially pure titanium (cp-Ti), was used, supplied by GoodFellow Ltd. (Cambridge, UK). The material was grade 2, with a high purity of 99.6%, and had been subjected to the annealing process. The as-received foil, 2.0 mm thick, was cut into discs of 15 mm in diameter. The surface of the cp-Ti specimens was prepared metallographically in two different ways, to compare the effect of roughness on the ALD deposition. For metallographic preparation the LaboPol-20 machine, as well as all the other equipment: grinding papers, polishing cloths and suspension, were supplied by Struers (Ballerup, Denmark). The first group of specimens was prepared by grinding, using 500-grit SiC emery papers, giving what is considered as a rough surface; the specimens were denoted as Ti-500. The second group of specimens was pre-

pared by similar grinding followed by polishing with silica suspension (OP-S) with SiO_2 particles, size 0.25 μm, with the addition of chemical reagents, 30% H_2O_2 and 25% NH_4OH (Merck KGaA, Darmstadt, Germany), according to Struers protocol. This procedure is known as chemical-mechanical polishing [44]. Specimens prepared in this way were considered as smooth and denoted as Ti-OPS. After metallographic preparation, both group of specimens were cleaned in 99.6% ethanol (Merck KGaA, Darmstadt, Germany) using an ultrasonication bath Elmasonic P series (Elma Schmidbauer GmbH, Singen, Germany) for 10 min, then dried with high pressure nitrogen gas. To ensure uniform surface conditions, i.e. comparable formation of a natural TiO_2 film, all the specimens were before the deposition processes stored overnight (ca. 16 h) in a vacuum desiccator filled with commercial silica gel. Additionally, Si-wafers with SiO_2 thermal oxide of 450 nm in thickness were used as perfectly smooth and control specimens.

2.2. Atomic layer deposition procedures

The ALD thin films were deposited using a Beneq TFS 200 system (Beneq Oy, Finland). Two types of thin films were deposited on cp-Ti specimens prepared as described in Section 2.1. Aluminium(III) oxide (Al_2O_3 or alumina) was deposited using trimethylaluminium ($Al(CH_3)_3$ or TMA, 99.99% PURATREM, STREM Chemicals Inc.) as the precursor. Hafnium(IV) oxide (HfO_2 or hafnia) was deposited using tetrakis(ethylmethylamido)hafnium(IV) ($Hf[N(CH_3)(C_2H_5)]_4$ or TEMAH, 99.99% PURATREM, STREM Chemicals Inc.) as precursor. For both types of thin films, Milli-Q water (resistivity 18 MΩ cm^2 at 25 °C, Billerica, MA) was used as the oxidizing agent. The Al_2O_3 films were deposited at 160 °C, and the HfO_2 films at 180 °C, according to the procedures for 100 nm thick films, as follows: in the case of alumina, the ALD cycle consisted of a 0.35 s TMA dose, a 1 s N_2 purge, a 0.3 s water dose and a 1 s N_2 purge; in the case of hafnia, the ALD cycle consisted of a 0.5 s TEMAH dose, a 1 s N_2 purge, a 0.2 s water dose and a 1 s N_2 purge. The number of deposition cycles was calculated using a growth rate per cycle (GPC) of 1 Å/cycle in the case of Al_2O_3 film, meaning that 1000 cycles would result in a 100 nm thick film. In the case of HfO_2 film the GPC was 0.96 Å/cycle, and 1050 cycles were used to obtain ca. 100 nm thick film. However, the film thickness may vary by a few tens of nanometres on different surfaces, as shown below.

2.3. Characterization techniques

The thicknesses of the ALD films were determined, using the ellipsometry method with an imaging ellipsometer Nanofilm_ep3se (Accurion GmbH, Goettingen, Germany). The specimens were illuminated with a laser beam at a wavelength of 610 nm and the measurements performed using a range of incidence angles from 45° to 66°. The experimental data were fitted according to the Cauchy model to determine the thickness, using the EP4 modeling software of Accurion. Measurements were performed on Si wafers and on cp-Ti specimens in air. In the case of Si wafer the model used was as follows: crystalline Si (100) as substrate, then ca. 450 nm of deposited SiO_2 and the expected 100 nm of alumina and hafnia, respectively. In the case of Ti-OPS specimens, the model used was as follows: Ti metal as substrate, then 1–5 nm of naturally formed TiO_2 and the expected 100 nm of alumina and hafnia, respectively. However, in the case of the Ti-500 it was necessary to consider a relatively high surface roughness when choosing the model. Therefore, an effective medium approach was used taking into account that there are no clear borders at the inner interface between Ti and ALD film and at the outer interface between ALD film and air at the top surface, but their mixtures. The model that showed the best fit with the measured results and the smallest RMSE error was: Ti metal as substrate, mixture of Ti with alumina or hafnia and then mixture of alumina or hafnia with air. In this way, the thickness of the ALD films, alumina and hafnia, was estimated as the sum of the thicknesses of the two listed mixtures.

The results of thickness obtained by ellipsometry were compared with those obtained by depth profiles, using the ToF-SIMS depth profiles and SEM-FIB analysis of the cross-section (vide infra). It is noteworthy that the film thicknesses obtained by ellipsometry and the ToF-SIMS methods are based on measurement of a certain property of the thin film, then compared with the theoretical model and with the standard material, respectively. In contrast, in the SEM-FIB method thickness is measured directly, which gives much more reliable information.

3D surface imaging and the roughness of the prepared specimens were determined, by the stylus profilometry method, with a Bruker DektakXT profilometer. The radius of the stylus was 2 μm, and the applied force was 1 mg. 3D map resolution was 2 μm/trace and scanned on a surface area of 1 × 1 mm^2. Data were processed using Bruker Vision 64 and TalyMap Gold 6.2 software to create 3D surface topography and to calculate the mean surface roughness (S_a) as the average of the measurements on three different specimens. The parameter S_a is used generally to evaluate surface roughness of 3D profile, Eq. (1) [45].

$$S_a = \frac{1}{l_x}\frac{1}{l_y}\int_0^{l_x}\int_0^{l_y}|z|\mathrm{d}x\mathrm{d}y \tag{1}$$

Two spectroscopic methods, ToF-SIMS and EDXS, were employed with the aim of revealing the chemical composition of thin films. Compositional depth profiles of the thin films were obtained using ToF-SIMS 5 (IonToF, Germany). A pulsed Bi^+ primary ion source of 30 keV and 1 pA was delivered over a 50 × 50 μm^2 area to analyse the films. The pressure in the chamber was less than 10^{-9} mbar. Depth profiles were obtained by O^{2+} sputtering ion beams of 2 keV and 545 nA over a 400 × 400 μm^2 area in the case of alumina thin films and by Ar^+ sputtering ion beams of 2 keV and 380 nA over a 400 × 400 μm^2 area in the case of hafnia thin films. Characteristic signals related to the thin films, such as Al^+ and AlO^+ and Hf^+ and HfO^+, were collected during the analyses. Since the Si wafers were used for ToF-SIMS analyses as substrates, signals from Si^+ or SiO^+ were collected to determine the interface and thickness of the thin films. The comparison of the etching rates of the standard material, for which pure SiO_2 of known thickness was used, and the experimentally prepared ALD thin films deposited on a very smooth surface such as polished Si, gives an approximate value of the thin films thicknesses. Calibration of the ToF-SIMS instrument regarding the etching rate is commonly performed on the SiO_2 standard because its etching rate was shown to be approximately the same as for most metal oxide materials. Sputtering rates were determined on SiO_2 standard using different types of ion beams with different beam characteristics, as described above. Therefore, the sputtering rate determined on SiO_2 standard under the experimental conditions used for sputtering alumina and hafnia was 0.2 nm/s and 0.5 nm/s, respectively.

EDXS spectra were collected using an Oxford Instruments INCA system. Morphological characterization was performed using two types of scanning electron microscope (SEM), a JEOL JSM-7600 F and a Carl Zeiss EVO-40. Only polished specimens, at the top surface and at the cross-section sites, were used for the EDXS analysis. For ALD thin films analyses, a minimal beam acceleration voltage of 3 kV was used to avoid gathering information from the metal substrate and to focus the analysis primarily on the ALD films (ca. 100 nm in depth of the ALD films). At some areas of interest, a larger analysis depth of ca. 3 μm (achieved by a beam acceleration voltage of 10 kV) was used to obtain information on both the thin

Table 1
Chemical composition of the Hanks' solution.

Components	Concentration/ g L^{-1}
NaCl	8.0
KCl	0.40
$NaHCO_3$	0.35
$CaCl_2$	0.14
$MgCl_2 \cdot 6H_2O$	0.10
$MgSO_4 \cdot 7H_2O$	0.06
$Na_2HPO_4 \cdot 2H_2O$	0.06
KH_2PO_4	0.06
Glucose	1.0

film and the underlying substrate. Although EDXS analyses provided results as the relative atomic ratio between Al or Hf and O atoms, they should be considered as being semi-quantitative, since the EDXS instrument was not calibrated specifically for the alumina and hafnia ALD thin films. The same conditions were used for the cross-section analysis. In general, 3 kV beam acceleration voltage was sufficient to obtain useful results.

SEM imaging was performed at beam acceleration voltages from 1 kV to 5 kV using an ETD detector and upper (SEI) and lower (LEI) detectors of secondary electrons (SE) to obtain insights into the morphology of the surface. A CBS and a LABE detector for back-scattered electrons (BSE) were used to get information on the composition, since they provide a contrast between areas with different chemical compositions. In addition to surface images, cross-section images were also taken to check the homogeneity and thickness of the films. Prior to SEM imaging and EDXS analyses, one half of both specimens, alumina and hafnia coated cp-Ti, were coated with a thin Pt protection layer and the other half with a thin carbon layer to reduce the charging effect while acquiring information from the surface.

Cross-section surfaces were obtained using a FIB FEI Helios 650 Nanolab instrument with Ga^+ as etching beam. Prior to analysis, a 1 μm thick Pt protective layer was deposited over the cross-section site as an additional protective layer. The cross-section was then made by rough etching of ALD thin films followed by fine polishing using a lower current.

Considering the nanometric thickness of the films, only polished specimens were investigated by ToF-SIMS, EDXS and FIB techniques aiming to provide a very sharp interface substrate/ALD film, and, consequently, more accurate and precise characterization by individual technique than on the rough specimens.

2.4. Electrochemical measurements

All electrochemical measurements were performed using a potentiostat/galvanostat with electrochemical impedance modulus, Autolab PGSTAT302N (Metrohm AG, Herisau, Switzerland), and controlled by Nova 2.1.4 software. The standard configuration with three electrodes was used with an Ag/AgCl (3 M KCl) electrode (E = 0.192 V vs. standard hydrogen electrode) as the reference electrode and a carbon rod as the counter electrode. The specimen set in a Teflon holder with an area of 1 cm^2 exposed to the electrolyte solution served as a working electrode. All the potentials in the text are given with respect to the Ag/AgCl electrode. With the aim of simulating human body conditions, the electrochemical tests were performed in an Autolab 400 mL corrosion cell thermostated at 37 ± 0.1 °C, with Hanks' solution as the electrolyte with a pH of 7.4. Hanks' solution is a recommended and well-known simulated body fluid (SBF) solution (Table 1) [46]. All chemicals used for the preparation of the electrolyte were of *p.a.* purity and were supplied by Merck (Darmstadt, Germany) and Sigma-Aldrich (St. Louis, Missouri, USA).

Potentiodynamic polarization (PDP) and electrochemical impedance spectroscopy (EIS) measurements were performed on both bare and coated specimens. Polarization curves were obtained using a scan rate of 1 mV/s, starting at −0.25 V vs. open circuit potential (OCP) up to 4.0 V. Prior to measurements, specimens were allowed to rest for 1 h at the OCP. The EIS measurements were performed in the range from 100 kHz to 1 mHz with an AC excitation voltage of 10 mV (rms), resulting in 7 points per frequency decade. The measurements were carried out after specific immersion times at the OCP: 1 hour, 1 day, 5 days, 15 days and 40 days.

Electrochemical parameters (corrosion potential, E_{corr}, corrosion current density, j_{corr}, and polarization resistance, R_p) were determined from PDP curves in order to evaluate the electrochemical porosity of ALD films on differently prepared cp-Ti surfaces. The polarization resistances were calculated using the Stern-Geary equation (Eq. (2)).

$$R_p = \frac{B}{j_{corr}} = \frac{|b_a| \cdot |b_c|}{2.3 \cdot (|b_a| + |b_c|) \cdot j_{corr}} \quad (2)$$

where B is the Stern-Geary constant, and b_a and b_c are the slopes of the anodic and cathodic branches of the Tafel plots. For uncoated substrates, the value of j_{corr} was determined as the intersection of tangents to cathodic and anodic branches. For coated substrates, the j_{corr} value was determined as the intersection of the tangent to the anodic branch and the line through the E_{corr}.

There are several methods for calculating thin film porosity (P) [47] but, in electrochemistry, mainly the simple Eq. (3), introduced by Tato and Landolt, is used [48]. This equation corresponds to the ratio of the polarization resistances of the bare (R_p) and coated substrates ($R_{p,ALD}$).

$$P = \frac{R_p}{R_{p,ALD}} \cdot 100 \quad (3)$$

Later, this equation was complemented, in the study by Liu and co-workers, to Eq. (4) [49], and used in many recent papers to describe the porosity of physical and chemical vapor deposition (CVD) films to be used as protection against corrosion [37,47,50,51]. The total porosity of the coating (P) determined using Eq. (4) takes into account other electrochemical parameters:

$$P = \frac{R_p}{R_{p,ALD}} \cdot 10^{-\left(\frac{\Delta E_{corr}}{b_a}\right)} \cdot 100 \quad (4)$$

where ΔE_{corr} is the difference in the corrosion potentials between the bare and coated cp-Ti surfaces, $\Delta E = |E_{corr}$ - $E_{corr,ALD}|$, and b_a refers to the anodic Tafel slope of the bare cp-Ti substrate. In the present work, P was calculated using both equations, Eqs. (3) and (4).

The data of PDP curves presented for the coated specimens have been smoothed (using the FFT filter in Origin®) in order to remove the high level of noise detected for such low current values, close to the detection limit of the equipment.

3. Results and discussion

3.1. Surface morphology

The 3D surface profiles of ground (Ti-500) and polished (Ti-OPS) specimens were obtained using the profilometry method. Differences in roughness, expressed as S_a values, of ground and polished specimens, were relatively high. The range of S_a was 200 nm in the case of ground specimens, while polished specimens, with very smooth surfaces, had S_a values in the range of 10 nm, i.e. one order of magnitude smaller (Fig. 1a–f).

As has been proved previously, the main feature of the thin films grown by ALD is that they follow, almost perfectly, the topography of the substrate surface [31,32]. This property stands out,

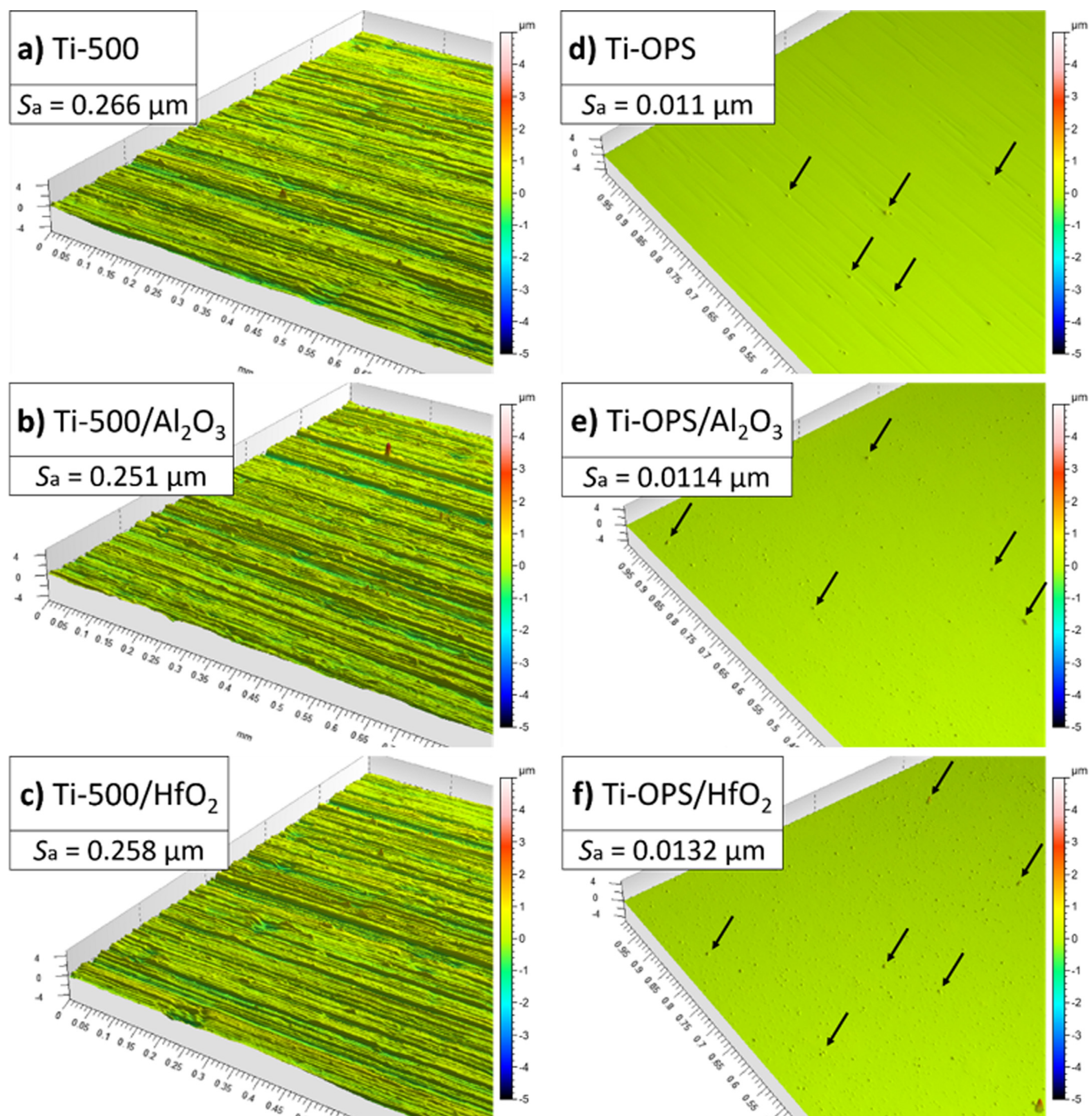

Fig. 1. 3D surface profiles of differently prepared bare and coated specimens of cp-Ti and their roughness values (S_a) obtained by profilometry, a) bare ground cp-Ti surface; b) ground cp-Ti surface coated with alumina; c) ground cp-Ti surface coated with hafnia; d) bare, polished cp-Ti surface; e) polished cp-Ti surface coated with alumina; f) polished cp-Ti surface coated with hafnia. Arrows in polished specimens denote the spots from which the SiO_2 particles were removed.

especially for certain films such as alumina, which tend to form an amorphous structure with a smooth surface [23,32]. Some other films, such as hafnia, show the possibility of forming a certain amount of polycrystalline structure, which can result in an increase of roughness due to the growth of facets on the crystallites [37,40]. Here we observed that both ground (Fig. 1a–c) and polished (Fig. 1d–f) surfaces retained their roughness after deposition of the two ALD thin films since the S_a values, before and after depositions, differed negligibly. Accordingly, hafnia grown at the relatively low temperature of 180 °C probably does not show the very high crystallinity that would cause a significant increase in the roughness [40]. Moreover, the roughness, after deposition of both thin films on ground surfaces, was slightly decreased, confirming a smoothing effect [52,53]. Some irregularities (tiny bumps noted by arrows in Fig. 1d–f) were noticed on polished surfaces. It will be shown below that these features, caused by the removal of SiO_2 particles during sample preparation, could theoretically be a trigger for crystallite or agglomerate formation, in particular for hafnia.

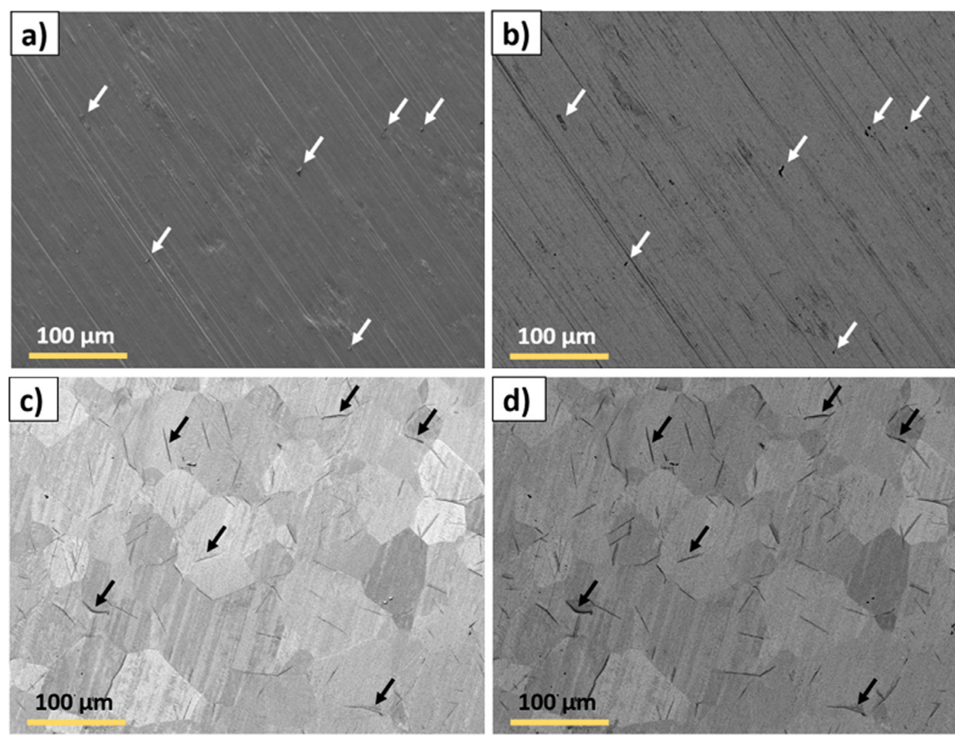

Fig. 2. SEM images of ground and polished cp-Ti surfaces from the a) secondary electrons (LEI detector) and b) backscattered electrons (LABE detector) showing the morphology and composition of the ground cp-Ti surface, c) secondary electrons and d) backscattered electrons, each showing the morphology and composition of the polished cp-Ti surface. White arrows denote SiC particles embedded in the ground cp-Ti surface; black arrows denote oxygen-rich areas on the polished cp-Ti surface. Magnification was 250 × and beam acceleration voltage 5 kV.

Comparison of the SEM images of the ground and polished cp-Ti surfaces shows a significant difference in the surface morphology (Fig. 2). Ground specimens exhibit a rough surface with random longitudinal scratches (Fig. 2a and b). In contrast, surface can be polished very well using the method described in Section 2.1, so that grains can be clearly seen in the SEM image (Fig. 2c and d). The microstructure is typical of coarse-grained titanium, with relatively large grains of several tens of micrometres. This means that the mechanical properties of cp-Ti were not affected by machining processes, as occurs in cases of severe plastic deformation, which was reported to lead to the breakdown of the coarse grains into ultra-fine or nano-sized grains [54–56]. H_2O_2 and NH_4OH added to the OP-S polishing suspension improve the removal rate of the ground titanium surface thus producing a reproducible, mirror-like surface appearance [44,57,58]; however, the surface can slightly differ in degree of polishing due to different removal (etching) rate and/or grain orientation. This may consequently produce a non-perfectly smooth surface at grain boundaries. The polished specimens combined action of H_2O_2 and exhibit increased hydrophilicity of the surface [59], which is necessary for uniform growth of ALD films [60].

The interaction between cp-Ti and the mixture of H_2O_2 and NH_4OH during the polishing allows successive chemical dissolution and oxidation of the titanium surface. Enlarged SEM image of grains on cp-Ti surface is presented in Fig. 3a and the corresponding EDXS analysis of different spots on the surface is given in the table in Fig. 3b. Surface is covered by a titanium oxide layer as the main constituents of the surface are titanium and oxygen. Some longitudinal sites are slightly richer in oxygen (spectra 1 and 3). Note that at smaller magnification these spots are observed as black lines in Fig. 2c and d. The formation of oxygen-rich areas can be related to the literature data reporting that the action of H_2O_2 and NH_4OH reagents during polishing results in the formation of Ti peroxide [59,61,62] and, even, the formation of superoxide [59]. The formation of Ti peroxide over the entire surface of cp-Ti could provide surface protection and improve the biocompatibility of the cp-Ti surface [59,61,62]. However, from the aspect of researching the barrier properties of ALD thin films, it is not of great importance, since the entire cp-Ti surface is covered with ALD film anyway.

At some spots on ground specimens residues of SiC particles embedded in the surface were observed (white arrows in Fig. 2a and b). In the case of polished specimens, however, several other features were evident (Fig. 2c and d). Cp-Ti is a soft and ductile metal whose surface is susceptible to deformation by the action of hard particles from grinding and polishing treatments. These particles can also be embedded in the surface, as reported [63]. The polishing processes predominantly remove the embedded SiC particles originating from the emery papers or of SiO_2 particles originating from the polishing suspension. Only some isolated particles were detected on the specimen surface (Fig. 3c). Several unrelated particles, ascribed to contamination, were also detected on the surface, although very rarely. The much smaller SiO_2 particles could be very tightly embedded in the surface, remaining there after rinsing with distilled water and ultrasonication in ethanol. However, thanks to the polishing procedure and extensive ultrasonic cleaning, SiO_2 particles were removed effectively from the surface, but dents and holes of regular circular shape remained at such spots (Fig. 3d). These features are noted by arrows on 3D surface profiles in Figs. 1d-e.

On coated samples, the dents and holes represent the sites, i.e. defects and edges, where agglomerates are formed during ALD process and could affect the growth of the ALD films and cause the formation of crystallites [40]. This is investigated further by SEM analysis. Agglomerates of nanometre size (denoted by white arrows) can be observed clearly over the entire surface (Fig. 4a and

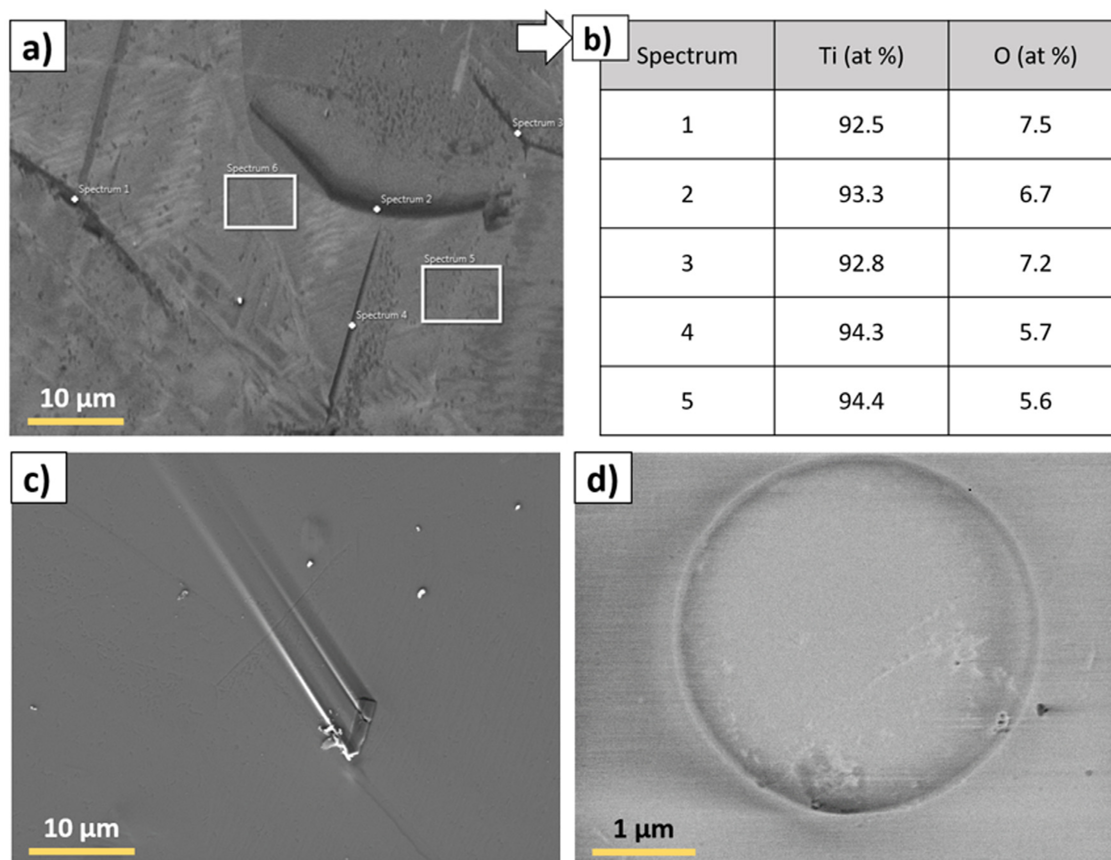

Spectrum	Ti (at %)	O (at %)
1	92.5	7.5
2	93.3	6.7
3	92.8	7.2
4	94.3	5.7
5	94.4	5.6

Fig. 3. a) SEM image of polished cp-Ti surface, recorded using the back-scattered electrons (LABE detector), magnification was 2000 ×, and b) chemical composition determined by EDXS analysis on numerated spots in SEM image in a). SEM images showing the morphology of c) embedded SiC particles in the Ti-OPS surface coated with alumina, recorded using the secondary electrons (LEI detector); magnification was 2300 ×, and d) of the site of the removed SiO_2 particle, recorded using the secondary electrons (SEI detector); magnification was 22,000 × . The beam acceleration voltage was 5 kV for all presented images.

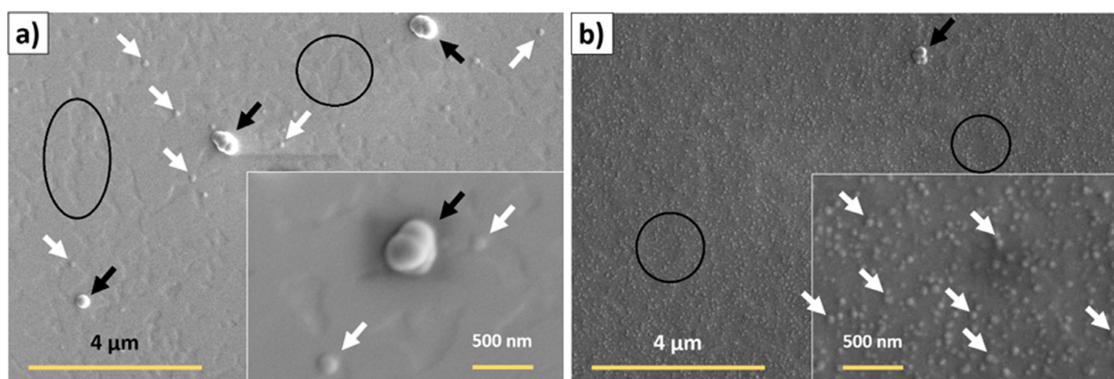

Fig. 4. SEM images recorded using secondary electrons (standard ETD detector), of a) alumina and b) hafnia thin films deposited on the Ti-OPS surface. Magnification was 10,000 × and 50,000 × (insets) and beam acceleration voltage 2 kV. White arrows denote ALD agglomerates or crystallites, black arrows denote larger contaminant particles, and black circles denote irregular features grown on oxygen-rich sites of the substrate (Fig. 3a,b).

b). This is much more noticeable in the case of the hafnia thin film (Fig. 4b), where the amount of very small agglomerates present on the surface was very large compared with that of alumina (insets in Fig. 4a). Accordingly, it has been concluded that the agglomerates are related mainly to tendency of hafnia to form a certain proportion of the crystalline phase in the film. As these features are not crucial herein, they are described a bit more in details in the Supplemental material; these issues will be investigated further in our next study. Contaminant particles formed due to transport and sample handling are denoted with black arrows (Fig. 4). Irregular features, several micrometres of length, were observed throughout the surface (denoted using black circles). They are formed on both alumina and hafnia thin films but were more visible on the former due to the less ALD agglomerates present. We believe that these irregular features are related to the growth of ALD films on oxygen-rich sites and/or grain boundaries, as described in Figs. 2 and 3a,b.

3.2. Chemical composition and thickness

The interfaces between ALD thin films and polished Si substrates can be clearly observed on the compositional depth profiles obtained by the ToF-SIMS technique. Due to the high level of

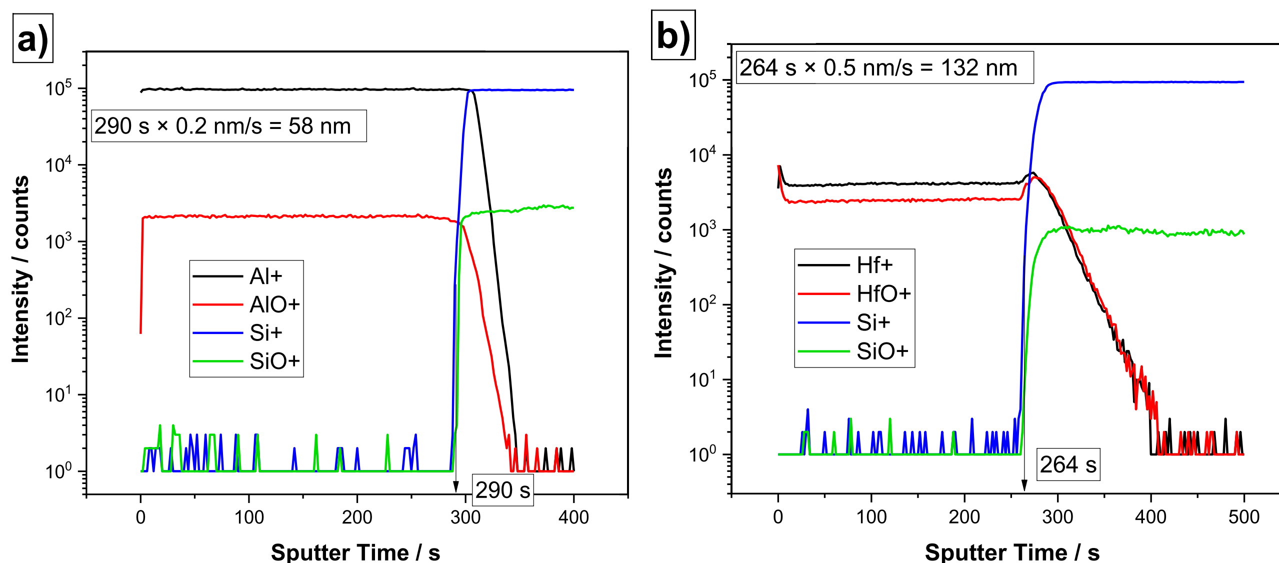

Fig. 5. Compositional depth profiles with calculation of the thickness of a) the alumina ALD thin film with the characteristic signals of Al^+ and AlO^+ and b) the hafnia ALD thin film with the characteristic signals of Hf^+ and HfO^+. Characteristic signals of Si substrates are Si^+ and SiO^+ ions.

smoothness of the polished Si wafers, this border is sharp enough to allow the estimation of the thin film thickness as described in Section 2.3. Signals for Al^+ and AlO^+ for alumina (Fig. 5a) and Hf^+ and HfO^+ for hafnia thin film (Fig. 5b) are shown. Si^+ and SiO^+ were used as the signals of the substrate. The ToF-SIMS depth profiling is a very useful method for analysing thin films, but the ratio of different ion intensities does not provide quantitative information on thin film [64]. Thus, due to the large variation in ionization probabilities between different chemical elements and compounds, SIMS can only be considered as a qualitative method. In the compositional profiles the difference is obvious. Al, as a relatively light element, can be very easily ionized in Al_2O_3 compound, where it gives an abundance of positive ions, while Hf, which is known as a hard metal, shows much poorer ionization, by more than one order of magnitude, in the HfO_2 compound (Fig. 5).

When considering the thickness of ALD thin films we cannot rely solely on the GPC and number of cycles because on substrates of different chemistry and roughness the ALD films can have a different growth rates and different densities or compactness. A thickness of 100 nm was expected according to the recipe developed previously on perfectly polished Si wafer samples. However, it has been proven in this study that on the polished cp-Ti the thickness can vary significantly and deviate from the expected one. Also, shortcomings of different methods when determining the thickness were detected and reliable thickness results were only obtained by direct measurement using SEM analysis at the cross-section site, which is described below.

In order to estimate the thicknesses of ALD thin films, the time at which an intensive increase in Si^+ signal occurred was taken as the indication that the interface has been reached (Fig. 5). Etching rates were ca. 0.2 nm/s for alumina and ca. 0.5 nm/s for hafnia thin films, as described in Section 2.3. Based on the obtained parameters, the thickness of the ALD thin film can be calculated as a product of the time at which interface with silica substrate is reached and the etching rate (Fig. 5). Accordingly, the thickness of the ALD alumina would be ca. 58 nm and that of the ALD hafnia film ca. 132 nm. These results in both cases show a large deviation from the expected thickness of 100 nm. This is because the ALD alumina thin film is amorphous, unlike the SiO_2 standard which is crystalline, so that specific calibration of the ToF-SIMS instrument should be performed using a standard of amorphous alumina film of exactly known thickness. A more suitable standard should also be taken for hafnia thin film. The similar problem with ALD thin films was observed in another study, where the glow discharge optical emission spectroscopy technique was used for estimating thickness [34].

Ellipsometry was taken as the second method for thickness evaluation. Like ToF-SIMS, it also gave non-reliable results at least for cp-Ti specimens. So, in the case of coated Si wafer, the thickness values were generally around 100 nm, but in the case of cp-Ti specimens this was not the case. The obtained values were 108 nm (±1 nm) for alumina and 109 nm (±1 nm) for hafnia thin films on Ti-OPS, which is very close to the expected value of 100 nm. However, the obtained root-mean-square-error (RMSE) values were 0.870 for alumina and 0.960 for hafnia, which indicates that the model does not fit good enough to the measured data, i.e. the obtained results may deviate from the actual thickness, which were significantly greater than 100 nm, as eventually determined at the cross-section of the thin films, using the FIB method (Fig. 6). By this method, the thickness of ca. 160 nm was measured for alumina (Fig. 6a) and ca. 150 nm for hafnia (Fig. 6b) thin films. These values were determined by taking into account the correction of the measured distance at the known angle of the electron beam. Note that the measured thickness may vary from site to site by a couple of nanometres due to the presence of agglomerates on the surface of the ALD films, especially in the case of hafnia. Fig. 6a and b are representative regarding the thickness of these ALD films, but do not show clearly the presence of agglomerates noticed especially in the case of hafnia film. Several further details are provided in Supplemental material (Figs. S1–S4) on films deposited on cp-Ti (Ti-OPS) and Si wafer substrates. However, a full characterization of the growth processes of different ALD films requires a more detailed study, which is beyond the scope of the present article.

Accordingly, the presented results emphasize that great care must be taken when determining the thickness, because evaluation based on a comparison of a certain property of the analysed and standard materials or of a theoretical model can result in an incorrect result, depending on the congruity of the analysed material with the selected standard material or theoretical model, respectively.

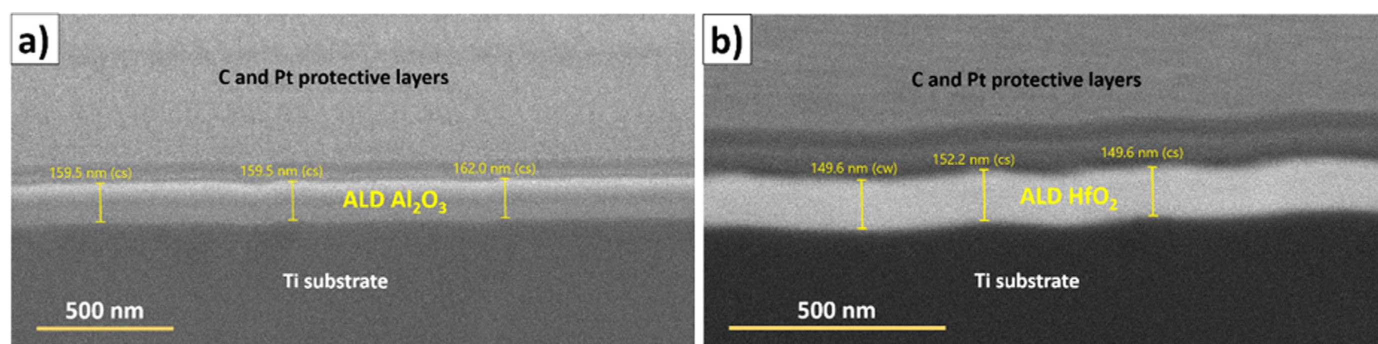

Fig. 6. SEM image, obtained by secondary electrons, of the ALD thin films on the cross-section sites of a) alumina and b) hafnia deposited on the polished cp-Ti surface. Magnification was a) 50,000 × and b) 80,000 × and beam acceleration voltage 2 kV.

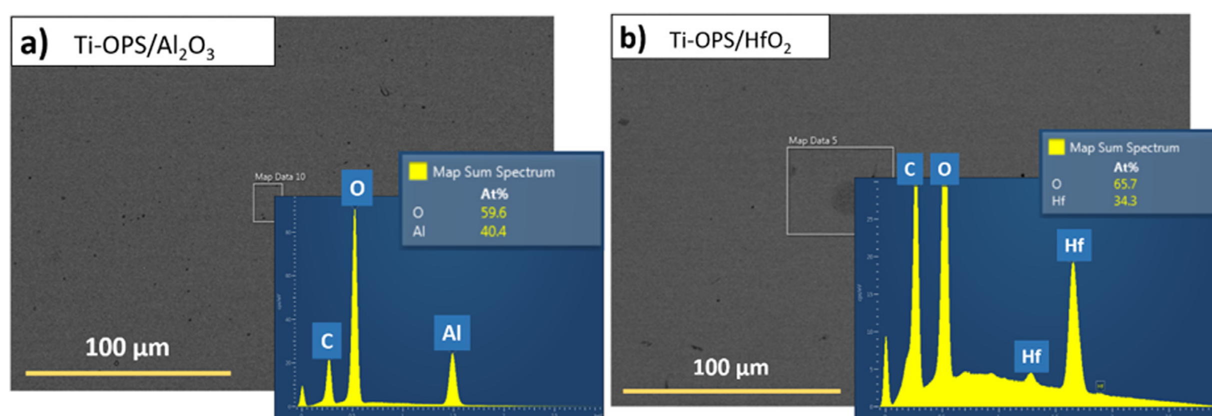

Fig. 7. SEM images, obtained from backscattered electrons (CBS detector), and EDXS spectra recorded on the surface of a) alumina and of b) hafnia ALD thin film on the polished cp-Ti surface. White rectangles at the SEM images are spots where EDXS analyses were made.

Regarding the rough surfaces, the specimens were not subjected to the FIB/SEM investigation to determine the thickness. Although ellipsometry cannot offer the exact thickness values, it can be used for relative thickness estimation, i.e. to estimate a ratio between thicknesses of ALD films on the smooth and rough surfaces, i.e. on the Ti-OPS and Ti-500 surfaces. Taking into account the surface roughness as described in Section 2.3, the thicknesses of both ALD films were up to 10 nm greater than those on smooth surfaces, 115 nm (± 1 nm) for alumina and 116 nm (± 1 nm) for hafnia. However, the RMSE values again showed a discrepancy between the measured data and the model, namely 0.578 for alumina and 1.575 for hafnia. Accordingly, we can only assume that the real ALD films thicknesses on the Ti-500 are somewhat thicker than those on the smooth Ti-OPS. This is also expected because ALD method tends to form thicker deposits on rough surfaces as proved here [37]. However, the precise thickness of these films is not the most important piece of information in this study, because it will be shown by electrochemical measurements that although having similar thicknesses, alumina and hafnia can exhibit different barrier properties on rough surfaces. It should be noted here that the ability of ellipsometry to measure the thickness of thin films on rough surfaces is highly questionable due to the depolarization of mirror-like reflected light [65]. Therefore, ellipsometry as a fast, efficient and non-destructive method was used only as an assistant method for estimating the thicknesses of these films.

The composition of the ALD films was determined using EDXS at the top surface (Fig. 7) and at the cross-section available to FIB (Figs. 8 and 9). EDXS analysis confirmed the chemical composition of both thin films (Fig. 7). Besides the pronounced peaks for O, and for Al and Hf, respectively, the strong peaks for C are also visible originating from the carbon thin films deposited to prevent the charging effect of the specimens, as explained in Section 2.3. Although this technique was not calibrated for the ALD thin films and should thus be considered as semi-quantitative, it can be stated that the experimental Al:O ratio is 2:3, in accordance with the stoichiometric ratio in alumina, and Hf:O is 1:2, as is expected for the stoichiometric ratio in hafnia (Fig. 7).

The FIB method allowed a cross-section of the thin films to be obtained and, subsequently, the EDXS analysis at the cross-section to be carried out (Figs. 8 and 9). In addition to the chemical composition, this provided very important information concerning the films' structure. SEM images show that both ALD films were compact and uniform, with no deformation sites or cracks (Figs. 8b and 9b). This visual information can be very clearly confirmed by EDXS analyses. No cracks or unexpected atoms were present in the thin film regions, but only Al, Hf and O atoms. EDXS mapping images confirmed the chemical composition (Figs. 8b and 9b). The observed overlapping of the signals of certain elements with others, especially for the hafnia thin film, is a consequence of contamination of certain layers with elements from adjacent layers during etching with Ga ions. However, it can be observed that ALD films follow the substrate surface, so there is no indication of delamination.

As already discussed in Section 3.1, EDXS revealed certain characteristics of the polished cp-Ti surface that are related to the effect of the combined action of H_2O_2 and NH_4OH (Fig. 2c and d). The SEM investigation of the polished cp-Ti surface covered with alumina ALD thin film revealed larger and smaller dark flecks or spots (Fig. 9). According to EDXS mapping analysis, these spots were found to be enriched in Ti and O atoms, indicating enhanced formation of passive TiO_2 film. As the second explanation, the possibility of thermally induced spreading of Ti peroxide during heat-

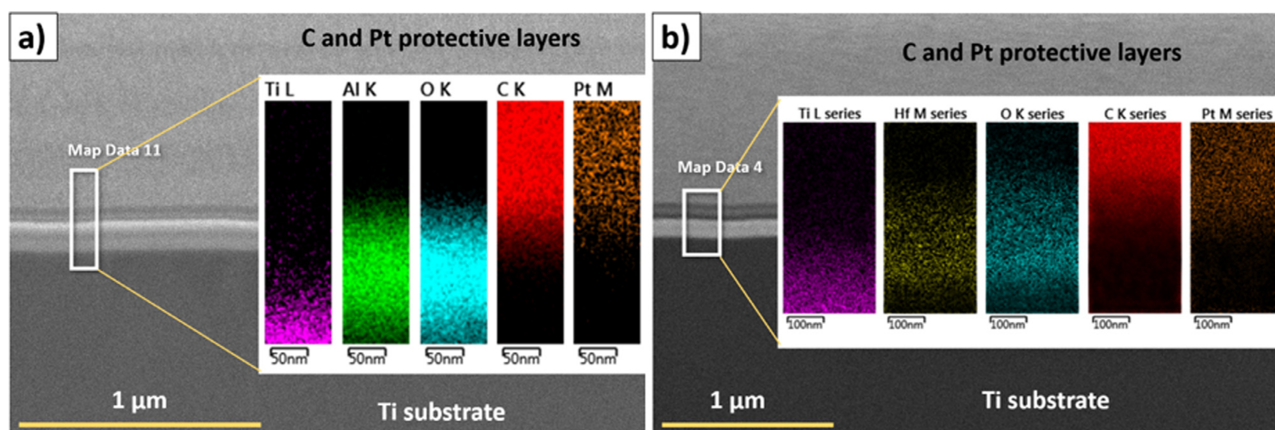

Fig. 8. SEM images of the cross-section site made by FIB of a) alumina and b) hafnia with EDXS mapping recorded at the white rectangle. SEM images were recorded using the secondary electrons under magnification of 40,000 ×; beam acceleration voltage was 2 kV.

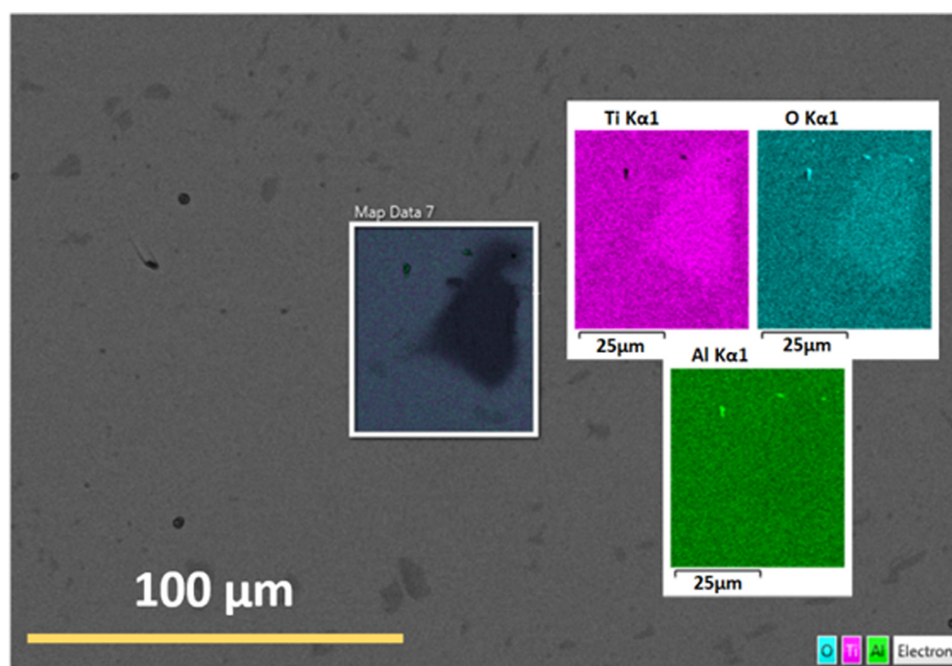

Fig. 9. SEM (BSE) images and EDXS mapping analysis recorded at the surface of alumina ALD thin film on the polished cp-Ti surface. Mapping was recorded within the white rectangles.

ing in the ALD chamber must be considered. Namely, since random sites enriched in oxygen on the uncoated polished surface (Fig. 3a and b) are ascribed to the formation of Ti peroxide, its growth and spreading could occur at increased temperatures before the ALD deposition. Although the formation of the Ti peroxide and its thermal treatment correlates with the improved protective properties of the cp-Ti surface and can help in the healing process after inflammation [61,62], its role under ALD thin film is negligible. But, what is more important in this study is that formation of oxide/peroxide below the ALD film does not affect the uniformity and compactness of the ALD films, as confirmed by the SEM investigation (Fig. 6).

3.3. Electrochemical properties

Potentiodynamic polarization (PDP) curves recorded for ground (Ti-500) and polished (Ti-OPS) bare cp-Ti samples following immersion of 1 h and 40 days at the open circuit potential (OCP) in Hanks' solution are presented in Fig. 10.

After 1 h of immersion, the current density increased exponentially from the corrosion potential up to ca. 0 V and −0.2 V for Ti-500 and Ti-OPS, respectively, when a broad passive plateau was established. At more positive potentials, the growth of highly insulating TiO_2 prevailed and continued up to 2.5 V and 2.8 V, when the current density increased due to oxygen removal from the layer [66,67]. According to the study that used XRD and XPS to characterize the passive layer on Ti-20Nb-10Zr-5Ta alloy as well as on pure Ti [68], the layer formed at lower potentials (up to 1 V) consists of a disordered mixture of amorphous Ti oxide and suboxide, i.e. TiO_2 and Ti_2O_3. On increasing the potential, it is completely transformed into a higher valence oxide, i.e. TiO_2. It can be concluded that the same process occurs here (Fig. 10), i.e. at 0 V and −0.2 V the passive film was transformed into amorphous TiO_2 which provided a broad, passive plateau of the current density. The formation of the crystalline TiO_2 passive film was reported to occur at higher potentials of ca. 5 V [66,69] and to be associated with breakdown of the passive film, but it was not observed here.

Table 2
Corrosion parameters and porosity of bare cp-Ti specimens and ALD coated specimens deduced from PDP curves recorded after 1 h immersion at the open circuit potential. Porosity was calculated, using Eqs. (3) and (4), from electrochemical parameters.

	E_{corr} / V vs Ag–AgCl	$\lvert\Delta E_{corr}\rvert$ / V vs Ag–AgCl	j_{corr} / A·cm^{-2}	R_p / Ω·cm^2	P/% (Eq. (3))	P/% (Eq. (4))
Ti-500	−0.561	–	4.7×10^{-8}	8.0×10^{5}	–	–
Ti-OPS	−0.421	–	1.4×10^{-8}	2.6×10^{6}	–	–
Ti-500/alumina	−0.549	0.012	2.3×10^{-11}	3.3×10^{8}	0.24	0.20
Ti-OPS/alumina	−0.445	0.024	3.5×10^{-11}	2.2×10^{8}	1.18	0.80
Ti-500/hafnia	−0.352	0.209	2.0×10^{-11}	6.3×10^{8}	0.13	0.05
Ti-OPS/hafnia	−0.273	0.148	1.1×10^{-11}	1.8×10^{9}	0.14	0.01

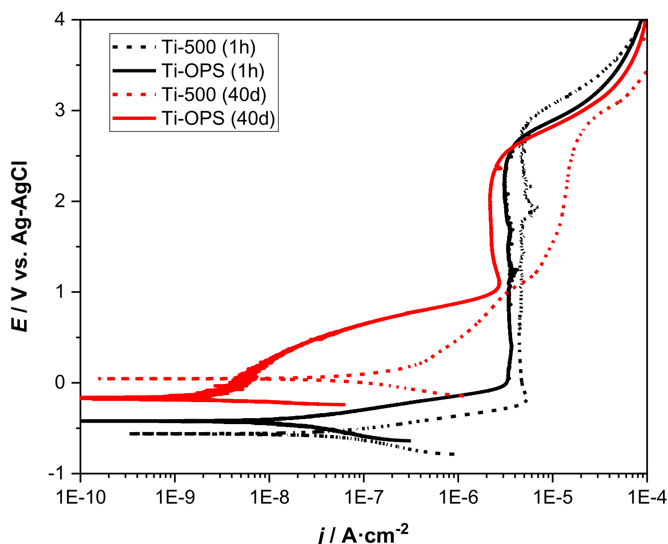

Fig. 10. Potentiodynamic polarization curves of bare ground and polished, Ti-500 and Ti-OPS, specimens recorded in Hanks' solution after 1 h and after 40 days of immersion at the open circuit potential. dE/dt = 1 mV/s.

There are notable differences in the values of electrochemical parameters measured after 1-hour immersion for Ti-500 and Ti-OPS (Fig. 10). Ti-OPS had about three times smaller j_{corr}, three times larger R_p and 0.1 V more positive E_{corr} than the Ti-500 specimen (Table 2). One of the reasons for this is the improved passivation of Ti-OPS due to chemical-mechanical polishing [61,62], as explained in Section 3.1. The other reason is the possibility of forming a less protective passive film on Ti-500 surface due to the stresses in the film on the rough surface; a similar feature has been investigated [70]. The appearance of stresses in the passive film would certainly make the metal more sensitive to the attack of corrosive species from Hanks' solution. Thus, Ti-OPS shows better corrosion resistance under simulated conditions of the human body *per se*.

After 40 days immersion of Ti-500 and Ti-OPS specimens the E_{corr} values were shifted to more positive values, i.e. by 0.6 V and 0.25 V, respectively (Fig. 10). This indicates that, after prolonged immersion, the oxide film in both cases contributed to the surface passivation. The strong shift of the Ti-OPS curve to smaller current density and more positive potentials may be related to the presence of the Ti-peroxide gel, as well as to the formation and continuous growth of the mixture of oxides and suboxides in the passive film during 40 days. The increase in the current density was completely halted at potentials below 1 V. At more positive potentials the long-immersed Ti-OPS specimen showed the same characteristics as that after 1 h of immersion, i.e. the passive film was completely transformed into TiO_2. In the case of Ti-500, the j_{corr} increased slightly at prolonged immersion, an observation that will be interesting to compare with EIS results (vide infra). The shape of PDP curves was similar as at the beginning of immersion. So, on the Ti-500 specimen, which was initially not covered by the Ti-peroxide gel, a disordered passive film was formed during 40 days, due probably to stresses present in the film on the rough surface, making it an inadequate insulation barrier for establishing a constant current density as was the case of Ti-OPS.

A significant reduction of j_{corr} values is evident for all ALD-coated cp-Ti specimens following immersion for 1 hour at the OCP (Fig. 11). Alumina coated cp-Ti specimens showed much smaller j_{corr}, by ca. three orders of magnitude, compared to uncoated specimens (Table 2). The R_p values increased accordingly. It is worth noting that alumina thin films did not significantly alter the shape of the PDP curves of bare cp-Ti specimens, nor do the values of the E_{corr}, suggesting that the alumina does not show specific electrochemical activity (Fig. 11a), as expected regarding the ability of the ALD technique to form very conformable and dense ceramic thin films [31,32,37].

Unlike the thin films with alumina, those with hafnia showed a positive shift of E_{corr} after deposition on both Ti-500 and Ti-OPS specimens, of 0.2 V and 0.15 V respectively (Fig. 11). The hafnia ALD thin films have very rarely been investigated for anti-corrosive purposes. It was reported that hafnia provides a more negative E_{corr} than the substrate (Cu specimen) [37], as opposed to the results in the present study. Here it was shown that hafnia, as a high-κ gate dielectric material, provides additional electrical insulation of the cp-Ti surface and thus very good barrier properties.

Porosity calculated from electrochemical parameters using Eqs. (3) and (4) are given in Table 2. Hafnia generally shows lower porosity than alumina thin films regardless the equation used (Table 2). This difference in porosity between hafnia and alumina is particularly highlighted in the case of the Ti-OPS specimen, which can also be inferred from the PDP curves (Fig. 11). Hafnia reduced the value of j_{corr} by more than three orders of magnitude in the case of Ti-500, and even more in the case of the Ti-OPS specimen (Table 2). The R_p values increased accordingly, reaching values in the range of GΩ·cm^2. Since the values of R_p and ΔE (ΔE=|E_{corr} - $E_{corr,ALD}$|) are the basis for the calculation of porosity, the changes of these parameters are reflected in the final values (Table 2). Moreover, porosity is calculated in relation to the parameters of uncoated specimens, which means that polished samples generally have larger R_p values. The ΔE for HfO_2 coated samples is broader, consequently, the porosity will differ considerably depending whether Eq. (3) or Eq. (4) have been taken for the calculation (Table 2). All these factors result in different trends in porosity for alumina and hafnia coated samples. For alumina, the porosity is higher for polished samples regardless the equation used. This apparently higher porosity may be related to the fact that both alumina coated samples exhibit similar R_p values so the relative increase compared to uncoated substrate is smaller for polished sample (as P is calculated as ratio of R_p of bare and coated samples). Also note that alumina grows as an amorphous film and is difficult to crystallize, regardless of the surface irregularities [32]. Hafnia tends to be denser (or less porous) on the polished cp-Ti surface if the porosity is calculated taking into account the ΔE, i.e. using Eq. (4). In contrast, no difference in calculated porosity concerning

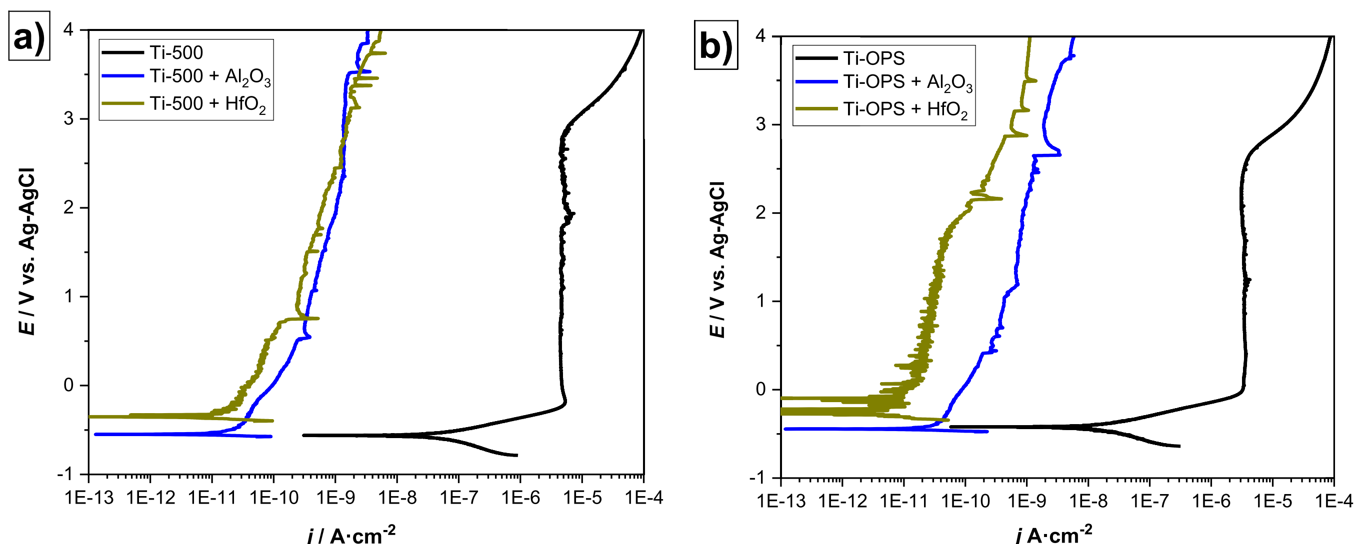

Fig. 11. Potentiodynamic polarization curves for bare and ALD coated cp-Ti specimens recorded in Hanks' solution after 1 h of immersion at the open circuit potential: a) ground, Ti-500, specimens and b) polished, Ti-OPS, specimens. dE/dt = 1 mV/s.

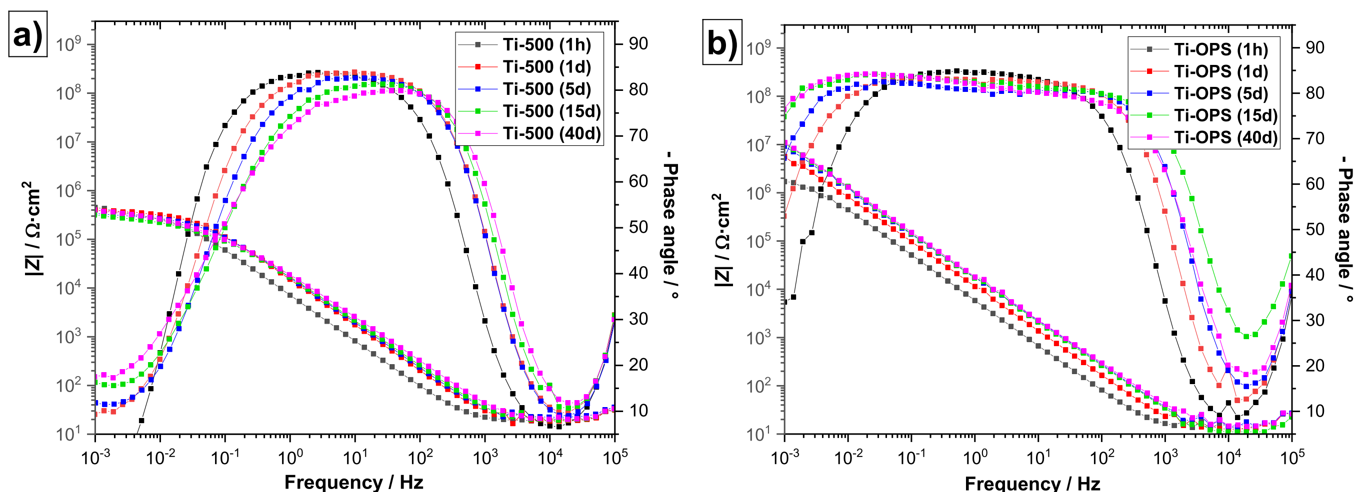

Fig. 12. Bode plots of bare cp-Ti specimens recorded over 40 days of immersion in Hanks' solution at 37 °C for a) ground cp-Ti and for b) polished cp-Ti specimen.

the surface roughness was observed if ΔE was excluded, i.e. using Eq. (3). Note also that the absolute R_p values for hafnia deposited on polished surface are higher than on rough surface (opposite to results for alumina), which indicates good protection properties, as will be shown below using EIS data.

As PDP curves showed that the investigated ALD films on ground and polished cp-Ti surfaces have excellent barrier properties and low porosity, the following step was to perform long term EIS measurements to monitor their barrier properties for a longer period of time (40 days). The uncoated cp-Ti specimens exhibited a significant difference in impedance and phase angle values during 40 days (Fig. 12). Unlike the Ti-500, which showed a slight decrease in the protective properties of passive film as the phase angle decreased in the mean frequency range (Fig. 12a), the Ti-OPS specimen showed a continuous increase in impedance as well as phase angle values (Fig. 12b). Thus, the Ti-OPS exhibited better anti-corrosive properties at the beginning of the test than the Ti-500, but also showed a continuous improvement of anti-corrosive properties. This is predominantly due to the progressive growth of the oxide layer [3,71], but also there is also a certain effect of formation of phosphate precipitates from the Hanks' solution on the surface [72,73]. Therefore, the chemical-mechanical pre-treatment of the cp-Ti surface can improve the passivation process significantly in Hanks' solution and/or increase the susceptibility to precipitation of phosphate species. Mechanical treatment alone, i.e. grinding, did not significantly improve the long-term passivation process and anti-corrosive properties. The EIS results (Fig. 12) can be correlated to PDP curves after 40 days immersion (Fig. 10); there is a partial improvement of anti-corrosive properties due to the increase in E_{corr} in the case of Ti-500, but j_{corr} was even slightly larger and a plateau of current density was not established at potentials above 1 V. This indicates that the protective properties of the passive film on Ti-500 were poorer than in the case of Ti-OPS specimen.

The results of EIS measurements on alumina (Fig. 13) and hafnia (Fig. 14) coated specimens indicate impedance values significantly higher than those of the bare specimens. The critical impedance at the lowest frequency of 0.001 Hz ($|Z|_{0.001\ Hz}$) were taken as values to be considered when evaluating the protective properties of these films (Fig. 15). $|Z|_{0.001\ Hz}$ of alumina coated Ti-500 was negligibly higher after 1 h of immersion than that of Ti-OPS but, after immersion of 40 days, this difference was more noticeable and was 0.2 order of magnitude in favor of the Ti-OPS (Fig. 13). For alumina coated Ti-500, the $|Z|_{0.001\ Hz}$ decreased up to the 10th day

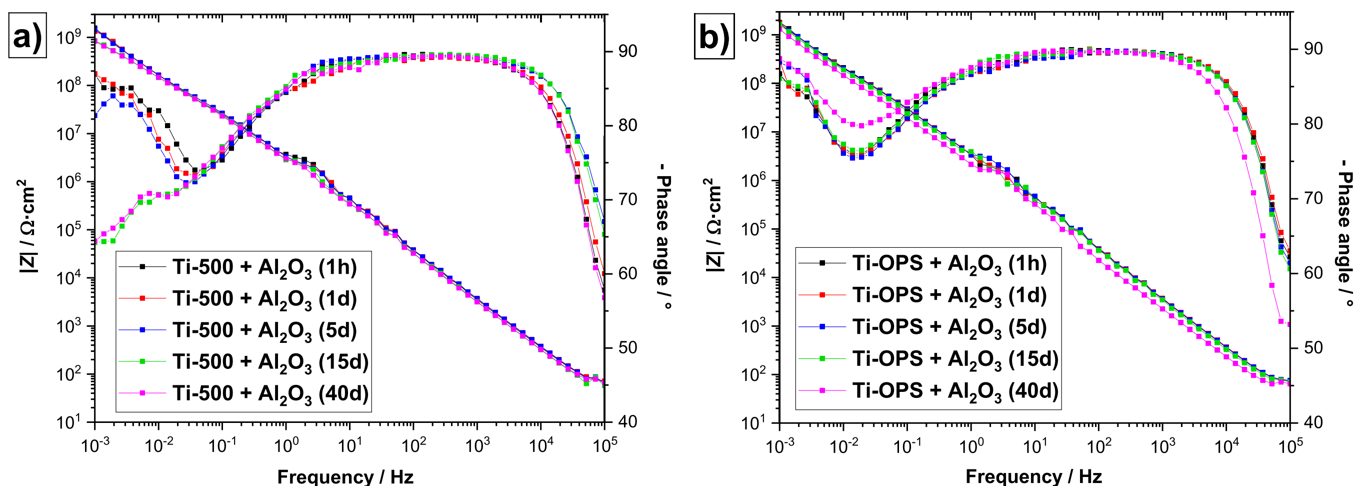

Fig. 13. Bode plots of alumina-coated cp-Ti specimens recorded during 40 days of immersion in Hanks' solution at 37 °C for a) a ground cp-Ti and b) a polished cp-Ti specimen.

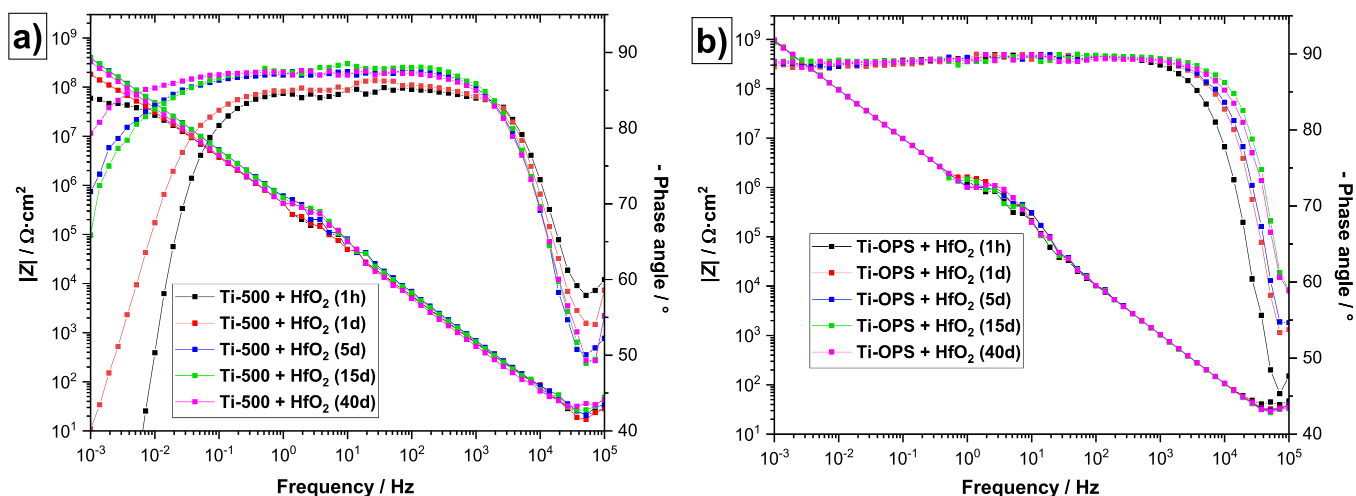

Fig. 14. Bode plots of hafnia-coated cp-Ti specimens recorded during 40 days of immersion in Hanks' solution at 37 °C for a) a ground cp-Ti and b) a polished cp-Ti specimen.

of immersion and then remained constant. What is also particularly noticeable is the phase angle drop after 15 days in the case of the Ti-500. This indicates the weakening of the film (Fig. 13a). In contrast, alumina coated Ti-OPS show stable impedance and phase angle values over 40 days (Fig. 13b). The alumina ALD thin film therefore retains its barrier properties slightly better on the polished cp-Ti surface.

In the case of hafnia coated specimens, this difference between Ti-500 and Ti-OPS was much more pronounced (Fig. 14). The $|Z|_{0.001\ \mathrm{Hz}}$ after immersion for 1 h was greater by more than one order of magnitude in favor of the Ti-OPS and, after immersion for 40 days, this difference was reduced (Fig. 15). This is due to a progressive increase in the impedance and phase angle values over 40 days in the case of Ti-500 (Fig. 14a). In fact, the response of impedance in these Bode diagrams looks very similar to that of the progressive passivation of bare polished metal surface (Fig. 12b). It can be concluded that the changes in Bode plots reflect the passivation of the cp-Ti surface through the pores of the film. The calculated porosity of the hafnia thin film is very low, i.e. 0.05% (Table 2), but it still appears to allow the additional passivation which is noticeable when considering the increase in phase angle during the immersion for 40 days (Fig. 14a). Unlike on the Ti-500, the hafnia on the Ti-OPS specimen showed much greater stability. The almost constant and very high impedance and the phase angle values over immersion for 40 days, are in accordance with its smaller porosity of only 0.01% (Fig. 14b, Table 2).

To summarize, both alumina and hafnia thin films on cp-Ti specimens exhibited high and stable $|Z|_{0.001\ \mathrm{Hz}}$ values, even after 40 days of immersion in Hanks' solution. However, differences exist regarding the substrate preparation (Fig. 15). Alumina thin film showed relatively good stability over immersion time, but with a continuously falling trend, especially when deposited on Ti-500. Hafnia thin film showed very good stability with continuously high $|Z|_{0.001\ \mathrm{Hz}}$ values only on the Ti-OPS. Comparison of the $|Z|_{0.001\ \mathrm{Hz}}$ for films on the Ti-OPS shows that alumina retained larger values but tended to fall slightly over 40 days, while hafnia had lower values but retained these with no indication of decay (Fig. 15). The superior behavior of hafnia is also indicated by the high and constant values of phase angles of −88°, even after 40 days immersion.

4. Conclusions

The ALD technique has been used as a means of depositing alumina and hafnia thin films on cp-Ti surfaces. The study had three main aims: (i) to characterize the thickness, composition and structure of deposited thin films, (ii) to characterize their electro-

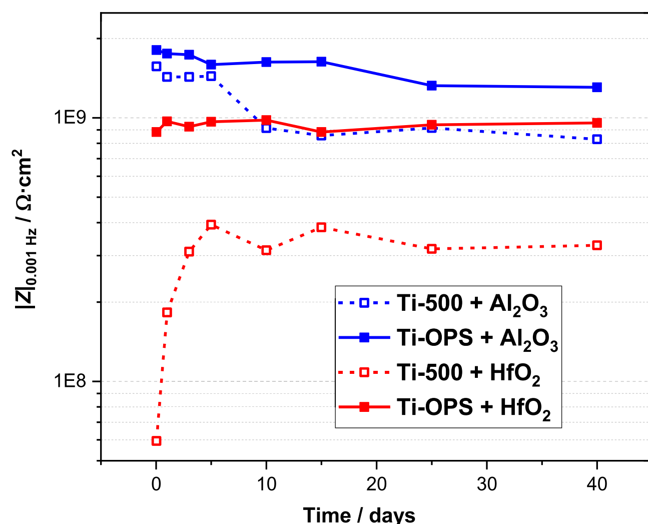

Fig. 15. Values of $|Z|_{0.001\ Hz}$ for ground and polished alumina and hafnia coated cp-Ti specimens as a function of immersion time in Hanks' solution at 37 °C.

chemical and corrosion properties in Hanks' simulated body fluid solution and (iii) to compare their properties as functions of the roughness of the substrate prior to deposition.

The uniform and very smooth surface of cp-Ti can be achieved only by using the silica suspension (0.25 μm gradation) and suitable chemical reagents or etchants (H_2O_2 and NH_4OH). Thanks to this procedure the surface is passivated, probably in the form of a Ti-peroxy gel, providing better corrosion protection than that of a ground surface with a naturally formed passive film. Both ALD thin films, alumina and hafnia, applied on rough and smooth cp-Ti surfaces, completely cover and perfectly follow the topography of the substrates. Therefore, the mean surface roughness after deposition on either ground or polished surface changes negligibly.

Potentiodynamic polarization curves show that both ALD thin films reduce significantly the corrosion current density of both ground and polished specimens, immediately after immersion in the electrolyte. Alumina provides similar corrosion protection of both rough and smooth surfaces while hafnia shows a notably greater reduction of corrosion current density on the smooth surface. In addition, unlike alumina, hafnia shows a certain electrochemical activity since it shifts the corrosion potential to ca. 0.2 V more positive values, thus appearing to inhibit the anodic reaction. EIS measurements show that both thin films when immersed in Hanks' solution for 40 days, exhibit, in general, a high capacitance character, with a broad region of linear increase in magnitude of the impedance and large values of phase angle. However, the variations in impedance response are dependent on the type of film and substrate pre-treatment. For alumina deposited on ground cp-Ti, the impedance magnitude at 10^{-3} Hz ($|Z|_{0.001\ Hz}$), which is taken as reflecting the barrier properties of the film, decreased until the 10th day of immersion and then remained constant. The reduction of $|Z|_{0.001\ Hz}$ is less for alumina on polished cp-Ti substrate and the film retains very high impedance values throughout the immersion period. On the other hand, EIS measurements of the hafnia thin film showed that it has excellent insulating properties on the polished surface, showing impedance values in the range of GΩ·cm^2 and a phase angle of −88° throughout the 40 days. However, on the ground surface, hafnia thin film shows increased electrochemical porosity, probably resulting in passivation of the Ti surface through the pores of the thin film. We assume that this may be related to the different proportion of crystallinity of hafnia grown on the ground and polished surface, with the former showing a larger content of crystalline phase, due to the irregularities present at the surface.

Regarding the ALD method itself, it was concluded that for the same ALD recipe, the thickness of alumina and hafnia thin films can vary significantly depending on the substrate. This depends on the chemistry of the surface, i.e. its reactivity for ALD reactions, but also on the uniformity of the surface because it is already known that ALD films on unordered surfaces tends to form less compact and consequently somewhat thicker films than it would be expected. Thus, the ALD recipe used here for 100 nm thick films resulted in significantly thicker films of ca. 160 nm in the case of alumina and ca. 150 nm in the case of hafnia.

The two techniques which in theory allow the determination of thickness, ToF-SIMS and ellipsometry, proved to be insufficient using the methodology applied. The only reliable result was obtained using the SEM analysis of the cross-section of the ALD film prepared by FIB method.

Declaration of Competing Interest

The authors declare that they have no known competing financial interests or personal relationships that could have appeared to influence the work reported in this paper.

Credit authorship contribution statement

Ivan Spajić: Methodology, Formal analysis, Data curation, Writing - original draft. **Peter Rodič:** Formal analysis, Writing - review & editing. **Gavrilo Šekularac:** Formal analysis, Writing - review & editing. **Maria Lekka:** Formal analysis, Methodology, Writing - review & editing. **Lorenzo Fedrizzi:** Methodology, Writing - review & editing. **Ingrid Milošev:** Conceptualization, Supervision, Methodology, Writing - review & editing.

Acknowledgments

This project has received funding from the European Union's Horizon H2020 research and innovation programme under the Marie Skłodowska Curie grant agreement No. 764977.

Financial support from the Slovenian Research Agency (research core funding Nos. P2-0393 and P1-0134) is acknowledged.

Access to scientific equipment (SEM/EDXS/FIB and ellipsometry) of the Centre of Excellence in nanoscience and nanotechnology – Nanocentre, Ljubljana is acknowledged.

The authors are grateful to Dr. Peter Panjan and Dr. Miha Čekada for help with profilometry measurements, to Dr. Janez Kovač for discussion of the ToF-SIMS results, to Dr. Luka Cmok and Dr. Matjaž Ličen for help with ellipsometry measurements and to Dr. Roger H. Pain for editing the manuscript.

Supplementary materials

Supplementary material associated with this article can be found, in the online version, at doi:10.1016/j.electacta.2020.137431.

References

[1] I. Milošev, Metallic materials for biomedical applications: laboratory and clinical studies, Pure Appl. Chem. 83 (2011) 309–324, doi:10.1351/PAC-CON-10-07-09.
[2] M. Niinomi, Recent metallic materials for biomedical applications, Metall. Mater. Trans. A 33A (2002) 477–486, doi:10.1007/s11661-002-0109-2.
[3] J. Pan, D. Thierry, C. Leygraf, Electrochemical impedance spectroscopy study of the passive oxide film on titanium for implant application, Electrochim. Acta 41 (1996) 1143–1153, doi:10.1016/0013-4686(95)00465-3.
[4] M. Niinomi, Mechanical biocompatibilities of titanium alloys for biomedical applications, J. Mech. Behav. Biomed. Mater. 1 (2008) 30–42, doi:10.1016/j.jmbbm.2007.07.001.

[5] M. Geetha, A.K. Singh, R. Asokamani, A.K. Gogia, Ti based biomaterials, the ultimate choice for orthopaedic implants – a review, Prog. Mater. Sci. 54 (2009) 397–425, doi:10.1016/j.pmatsci.2008.06.004.
[6] M. Kulkarni, A. Mazare, E. Gongadze, S. Perutkova, V. Kralj-Iglic, I. Milošev, P. Schmuki, A. Iglič, M. Mozetič, Titanium nanostructures for biomedical applications, Nanotechnology 26 (2015) 1–18, doi:10.1088/0957-4484/26/6/062002.
[7] R. Brånemark, P.I. Brånemark, B. Rydevik, R.R. Myers, Osseointegration in skeletal reconstruction and rehabilitation: a review, J. Rehabil. Res. Dev. 38 (2001) 175–181, https://pubmed.ncbi.nlm.nih.gov/11392650/.
[8] M. Niinomi, M. Nakai, Titanium-based biomaterials for preventing stress shielding between implant devices and bone, Int. J. Biomater. 2011 (2011) 1–10, doi:10.1155/2011/836587.
[9] M. Niinomi, Y. Liu, M. Nakai, H. Liu, H. Li, Biomedical titanium alloys with Young's moduli close to that of cortical bone, Regen. Biomater. 3 (2016) 173–185, doi:10.1093/rb/rbw016.
[10] ASTM F67-13 Standard Specification for Unalloyed Titanium, for Surgical Implant Applications (UNS R50250, UNS R50400, UNS R50550, UNS R50700), West Conshohocken, PA, 2017. https://doi.org/ 10.1520/F0067-13R17.
[11] C.N. Elias, D.J. Fernandes, C.R.S. Resende, J. Roestel, Mechanical properties, surface morphology and stability of a modified commercially pure high strength titanium alloy for dental implants, Dent. Mater. 31 (2015) e1–e13, doi:10.1016/j.dental.2014.10.002.
[12] R. Bhola, S.M. Bhola, B. Mishra, D.L. Olson, Corrosion in titanium dental implants/prostheses – a review, Trends Biomater. Artif. Organs 25 (2011) 34–46.
[13] R. Nishimura, J. Shirono, A. Jonokuchi, Hydrogen-induced cracking of pure titanium in sulphuric acid and hydrochloric acid solutions using constant load method, Corros. Sci. 50 (2008) 2691–2697, doi:10.1016/j.corsci.2008.06.037.
[14] R.B. Waterhouse, D.E. Taylor, Fretting debris and the delamination theory of wear, Wear 29 (1974) 337–344, doi:10.1016/0043-1648(74)90019-2.
[15] C.R. Ramos-Saenz, P.A. Sundaram, N. Diffoot-Carlo, Tribological properties of Ti-based alloys in a simulated bone-implant interface with Ringer's solution at fretting contacts, J. Mech. Behav. Biomed. Mater. 3 (2010) 549–558, doi:10.1016/j.jmbbm.2010.06.006.
[16] J.C.M. Souza, S.L. Barbosa, E. Ariza, J.P. Celis, L.A. Rocha, Simultaneous degradation by corrosion and wear of titanium in artificial saliva containing fluorides, Wear 292–293 (2012) 82–88, doi:10.1016/j.wear.2012.05.030.
[17] B. Sivakumar, L.C. Pathak, R. Singh, Role of surface roughness on corrosion and fretting corrosion behaviour of commercially pure titanium in Ringer's solution for bio-implant application, Appl. Surf. Sci. 401 (2017) 385–398, doi:10.1016/j.apsusc.2017.01.033.
[18] I. Milošev, From in vitro to retrieval studies of orthopedic implants, Corrosion 73 (2017) 1496–1509, doi:10.5006/2576.
[19] E. Marin, A. Lanzutti, F. Andreatta, M. Lekka, L. Guzman, Atomic layer deposition: state-of-the-art and research/industrial perspectives, Corros. Rev. 29 (2011) 191–208, doi:10.1515/CORRREV.2011.010.
[20] A.A. Malygin, V.E. Drozd, A.A. Malkov, V.M. Smirnov, From V. B. Aleskovskii's "Framework" Hypothesis to the Method of Molecular Layering/Atomic Layer Deposition, Chem. Vap. Depos. 21 (2015) 216–240.
[21] T. Suntola, J. Antson, Method for Producing Compound Thin Films, US4058430A, 1977. https://patents.google.com/patent/US4058430A/en.
[22] M. Leskelä, J. Niinistö, M. Ritala, Atomic layer deposition, in: Comprehensive Materials Processing, Elsevier Ltd., 2014, pp. 101–123, doi:10.1016/B978-0-08-096532-1.00401-5.
[23] R. Matero, M. Ritala, M. Leskelä, T. Salo, J. Aromaa, O. Forsén, Atomic layer deposited thin films for corrosion protection, J. Phys. IV 9 (1999) 493–499, doi:10.1051/jp4:1999862.
[24] J.A. Carlisle, M.J. Pellin, J.W. Elam, J. Wang, Hermetic Bio-Inert Coatings for bio-Implants Fabricated Using Atomic Layer Deposition, US2006/0251875A1, 2006. https://patents.google.com/patent/US20060251875.
[25] M.K. Abbass, S.A. Ajeel, H.M. Wadullah, Biocompatibility, bioactivity and corrosion resistance of stainless steel 316L nanocoated with TiO_2 and Al_2O_3 by atomic layer deposition method, J. Phys. Conf. Ser. 1032 (2018) 1–15, doi:10.1088/1742-6596/1032/1/012017.
[26] D.S. Finch, T. Oreskovic, K. Ramadurai, C.F. Herrmann, S.M. George, R.L. Mahajan, Biocompatibility of atomic layer-deposited alumina thin films, J. Biomed. Mater. Res. – Part A 87 (2008) 100–106, doi:10.1002/jbm.a.31732.
[27] Q. Yang, W. Yuan, X. Liu, Y. Zheng, Z. Cui, X. Yang, H. Pan, S. Wu, Atomic layer deposited ZrO_2 nanofilm on Mg-Sr alloy for enhanced corrosion resistance and biocompatibility, Acta Biomater. 58 (2017) 515–526, doi:10.1016/j.actbio.2017.06.015.
[28] I.P. Grigal, A.M. Markeev, S.A. Gudkova, A.G. Chernikova, A.S. Mityaev, A.P. Alekhin, Correlation between bioactivity and structural properties of titanium dioxide coatings grown by atomic layer deposition, Appl. Surf. Sci. 258 (2012) 3415–3419, doi:10.1016/j.apsusc.2011.11.082.
[29] M. Putkonen, T. Sajavaara, P. Rahkila, L. Xu, S. Cheng, L. Niinistö, H.J. Whitlow, Atomic layer deposition and characterization of biocompatible hydroxyapatite thin films, Thin Solid Films 517 (2009) 5819–5824, doi:10.1016/j.tsf.2009.03.013.
[30] V. Cremers, R.L. Puurunen, J. Dendooven, Conformality in atomic layer deposition: current status overview of analysis and modelling, Appl. Phys. Rev. 6 (2019) 1–35, doi:10.1063/1.5060967.
[31] M. Ritala, M. Leskelä, J.P. Dekker, C. Mutsaers, P.J. Soininen, J. Skarp, Perfectly conformal TiN and Al_2O_3 films deposited by atomic layer deposition, Chem. Vap. Depos. 5 (1999) 7–9 https://doi.org/1<7::AID–CVDE7>3.0.CO;2-J, doi:10.1002/(SICI)1521-3862(199901)5.
[32] M. Ritala, H. Saloniemi, M. Leskelä, T. Prohaska, G. Friedbacher, M. Grasserbauer, Studies on the morphology of Al_2O_3 thin films grown by atomic layer epitaxy, Thin Solid Films 286 (1996) 54–58, doi:10.1016/S0040-6090(95)08524-6.
[33] G.C. Correa, B. Bao, N.C. Strandwitz, Chemical stability of titania and alumina thin films formed by atomic layer deposition, ACS Appl. Mater. Interfaces 7 (2015) 14816–14821, doi:10.1021/acsami.5b03278.
[34] E. Marin, L. Guzman, A. Lanzutti, W. Ensinger, L. Fedrizzi, Multilayer Al_2O_3/TiO_2 atomic layer deposition coatings for the corrosion protection of stainless steel, Thin Solid Films 522 (2012) 283–288, doi:10.1016/j.tsf.2012.08.023.
[35] A.I. Abdulagatov, Y. Yan, J.R. Cooper, Y. Zhang, Z.M. Gibbs, A.S. Cavanagh, R.G. Yang, Y.C. Lee, S.M. George, Al_2O_3 and TiO_2 atomic layer deposition on copper for water corrosion resistance, ACS Appl. Mater. Interfaces 3 (2011) 4593–4601, doi:10.1021/am2009579.
[36] M.J. Biercuk, D.J. Monsma, C.M. Marcus, J.S. Backer, R.G. Gordon, Low-temperature atomic-layer-deposition lift-off method for microelectronic and nanoelectronic applications, Appl. Phys. Lett. 83 (2003) 2405–2407, doi:10.1063/1.1612904.
[37] J.S. Daubert, G.T. Hill, H.N. Gotsch, A.P. Gremaud, J.S. Ovental, P.S. Williams, C.J. Oldham, G.N. Parsons, Corrosion protection of copper using Al_2O_3, TiO_2, ZnO, HfO_2, and ZrO_2 atomic layer deposition, ACS Appl. Mater. Interfaces 9 (2017) 4192–4201, doi:10.1021/acsami.6b13571.
[38] Z. Fohlerova, A. Mozalev, Anodic formation and biomedical properties of hafnium-oxide nanofilms, J. Mater. Chem. B 7 (2019) 2300–2310, doi:10.1039/c8tb03180k.
[39] H. Matsuno, A. Yokoyama, F. Watari, M. Uo, T. Kawasaki, Biocompatibility and osteogenesis of refractory metal implants, titanium, hafnium, niobium, tantalum and rhenium, Biomaterials 22 (2001) 1253–1262, doi:10.1016/S0142-9612(00)00275-1.
[40] D.M. Hausmann, R.G. Gordon, Surface morphology and crystallinity control in the atomic layer deposition (ALD) of hafnium and zirconium oxide thin films, J. Cryst. Growth 249 (2003) 251–261, doi:10.1016/S0022-0248(02)02133-4.
[41] I. Milošev, Surface treatments of titanium with antibacterial agents for implant applications, in: S. Djokic (Ed.), Biomedical and Pharmaceutical Applications of Electrochemistry, Modern Aspects of Electrochemistry, 60, Springer, 2016, pp. 1–88, doi:10.1007/978-3-319-31849-3_1.
[42] R.A. Gittens, R. Olivares-Navarrete, Z. Schwartz, B.D. Boyan, Implant osseointegration and the role of microroughness and nanostructures: lessons for spine implants, Acta Biomater. 10 (2014) 3363–3371, doi:10.1016/j.actbio.2014.03.037.
[43] S.S. Santavirta, R. Lappalainen, P. Pekko, A. Anttila, Y.T. Konttinen, The counterface, surface smoothness, tolerances, and coatings in total joint prostheses, Clin. Orthop. Relat. Res. 369 (1999) 92–102, doi:10.1097/00003086-199912000-00010.
[44] S. Okawa, K. Watanabe, Chemical mechanical polishing of titanium with colloidal silica containing hydrogen peroxide – mirror polishing and surface properties, Dent. Mater. J. 28 (2009) 68–74, doi:10.4012/dmj.28.68.
[45] E.S. Gadelmawla, M.M. Koura, T.M.A. Maksoud, I.M. Elewa, H.H. Soliman, Roughness parameters, J. Mater. Process. Technol. 123 (2002) 133–145, doi:10.1016/S0924-0136(02)00060-2.
[46] H. Wang, R. Zhang, Z. Yuan, X. Shu, E. Liu, Z. Han, A comparative study of the corrosion performance of titanium (Ti), titanium nitride (TiN), titanium dioxide (TiO_2) and nitrogen-doped titanium oxides (N–TiO_2), as coatings for biomedical applications, Ceram. Int. 41 (2015) 11844–11851, doi:10.1016/j.ceramint.2015.05.153.
[47] S.H. Ahn, J.H. Lee, H.G. Kim, J.G. Kim, A study on the quantitative determination of through-coating porosity in PVD-grown coatings, Appl. Surf. Sci. 233 (2004) 105–114, doi:10.1016/j.apsusc.2004.03.213.
[48] W. Tato, D. Landolt, Electrochemical determination of the porosity of single and duplex PVD coatings of titanium and titanium nitride on brass, J. Electrochem. Soc. 145 (1998) 4173–4181, doi:10.1149/1.1838932.
[49] C. Liu, Q. Bi, A. Leyland, A. Matthews, An electrochemical impedance spectroscopy study of the corrosion behavior of PVD coated steels in 0.5 N NaCl aqueous solution: part II. EIS interpretation of corrosion behaviour, Corros. Sci. 45 (2003) 1257–1273, doi:10.1016/S0010-938X(02)00214-7.
[50] Z. Chai, J. Li, X. Lu, D. He, Use of electrochemical measurements to investigate the porosity of ultra-thin Al_2O_3 films prepared by atomic layer deposition, RSC Adv. 4 (2014) 39365–39371, doi:10.1039/C4RA04565C.
[51] B. Díaz, E. Härkönen, J. Świątowska, A. Seyeux, V. Maurice, M. Ritala, P. Marcus, Corrosion properties of steel protected by nanometre-thick oxide coatings, Corros. Sci. 82 (2014) 208–217, doi:10.1016/j.corsci.2014.01.024.
[52] J.W. Elam, Z.A. Sechrist, S.M. George, ZnO/Al_2O_3 nanolaminates fabricated by atomic layer deposition: growth and surface roughness measurements, Thin Solid Films 414 (2002) 43–55, doi:10.1016/S0040-6090(02)00427-3.
[53] W.S. Lau, J. Zhang, X. Wan, J.K. Luo, Y. Xu, H. Wong, Surface smoothing effect of an amorphous thin film deposited by atomic layer deposition on a surface with nano-sized roughness, AIP Adv. 4 (2014) 1–5, doi:10.1063/1.4866988.
[54] L. Mishnaevsky, E. Levashov, R.Z. Valiev, J. Segurado, I. Sabirov, N. Enikeev, S. Prokoshkin, A.V. Solov'Yov, A. Korotitskiy, E. Gutmanas, I. Gotman, E. Rabkin, S. Psakh'E, L. Dluhoš, M. Seefeldt, A. Smolin, Nanostructured titanium-based materials for medical implants: modeling and development, Mater. Sci. Eng. R Rep. 81 (2014) 1–19, doi:10.1016/j.mser.2014.04.002.
[55] G. Serra, L. Morais, C.N. Elias, I.P. Semenova, R. Valiev, G. Salimgareeva, M. Pithon, R. Lacerda, Nanostructured severe plastic deformation processed titanium for orthodontic mini-implants, Mater. Sci. Eng. C 33 (2013) 4197–4202, doi:10.1016/j.msec.2013.06.012.

[56] R.Z. Valiev, I.P. Semenova, V.V. Latysh, H. Rack, T.C. Lowe, J. Petruzelka, L. Dluhos, D. Hrusak, J. Sochova, Nanostructured titanium for biomedical applications, Adv. Eng. Mater. 3 (2008) 593–601, doi:10.1002/adem.200800026.

[57] D.V. Nazarov, E.G. Zemtsova, A. Yu. Solokhin, R.Z. Valiev, V.M. Smirnov, Modification of the surface topography and composition of ultrafine and coarse grained titanium by chemical etching, Nanomaterials 7 (2017) 1–15, doi:10.3390/nano7010015.

[58] C. Ohtsuki, H. Iida, S. Hayakawa, A. Osaka, Bioactivity of titanium treated with hydrogen peroxide solutions containing metal chlorides, J. Biomed. Mater. Res. 35 (1997) 39–47 https://doi.org/:1<39::AID−JBM5>3.0.CO;2-N, doi:10.1002/(SICI)1097-4636(199704)35.

[59] B. Wälivaara, B.O. Aronsson, M. Rodahl, J. Lausmaa, P. Tengvall, Titanium with different oxides: in vitro studies of protein adsorption and contact activation, Biomaterials 15 (1994) 827–834, doi:10.1016/0142-9612(94)90038-8.

[60] N.P. Kobayashi, C.L. Donley, S.Y. Wang, R.S. Williams, Atomic layer deposition of aluminum oxide on hydrophobic and hydrophilic surfaces, J. Cryst. Growth 299 (2007) 218–222, doi:10.1016/j.jcrysgro.2006.11.224.

[61] X. Liu, P.K. Chu, C. Ding, Surface modification of titanium, titanium alloys, and related materials for biomedical applications, Mater. Sci. Eng. R Rep. 47 (2004) 49–121, doi:10.1016/j.mser.2004.11.001.

[62] P. Tengvall, I. Lundström, L. Sjöqvist, H. Elwing, L.M. Bjursten, model studies of the influence of the inflammatory response on titanium implants, Biomaterials 10 (1989) 166–175, doi:10.1016/0142-9612(89)90019-7.

[63] O. Miyakawa, K. Watanabe, S. Okawa, M. Kanatani, S. Nakano, M. Kobayashi, Surface contamination of titanium by abrading treatment, Dent. Mater. J. 15 (1996) 11–21, doi:10.4012/dmj.15.11.

[64] J.C. Vickerman, I.S. Gilmore, Surface Analysis – The Principal Techniques, 2nd ed., Wiley, 2009, doi:10.1002/9780470721582.

[65] S.C. Siah, B. Hoex, A.G. Aberle, Accurate characterization of thin films on rough surfaces by spectroscopic ellipsometry, Thin Solid Films 545 (2013) 451–457, doi:10.1016/j.tsf.2013.07.067.

[66] C.K. Dyer, Breakdown and efficiency of anodic oxide growth on titanium, J. Electrochem. Soc. 125 (1978) 1032–1038, doi:10.1149/1.2131616.

[67] P.J. Boddy, Oxygen evolution on semiconducting TiO_2, J. Electrochem. Soc. 115 (1968) 199–203, doi:10.1149/1.2411080.

[68] I. Milošev, G. Žerjav, J.M. Calderon Moreno, M. Popa, chemical composition and thickness of passive film formed on novel Ti-20Nb-10Zr-5Ta alloy, Electrochim. Acta 99 (2013) 176–189, doi:10.1016/j.electacta.2013.03.086.

[69] J. Yahalom, J. Zahavi, Electrolytic breakdown crystallization of anodic oxide films on A1, Ta and Ti, Electrochim. Acta 15 (1970) 1429–1435, doi:10.1016/0013-4686(70)80064-0.

[70] C. Aparicio, F. Javier Gil, C. Fonseca, M. Barbosa, J.A. Planell, Corrosion behaviour of commercially pure titanium shot blasted with different materials and sizes of shot particles for dental implant applications, Biomaterials 24 (2003) 263–273, doi:10.1016/S0142-9612(02)00314-9.

[71] I. Milošev, M. Metikoš-Huković, H.H. Strehblow, Passive film on orthopaedic TiAlV alloy formed in physiological solution investigated by X-ray photoelectron spectroscopy, Biomaterials 21 (2000) 2103–2113, doi:10.1016/S0142-9612(00)00145-9.

[72] Y. Tanaka, E. Kobayashi, S. Hiromoto, K. Asami, H. Imai, T. Hanawa, Calcium phosphate formation on titanium by low-voltage electrolytic treatments, J. Mater. Sci. Mater. Med. 18 (2007) 797–806, doi:10.1007/s10856-006-0004-2.

[73] I. Milošev, J. Hmeljak, G. Žerjav, A. Cör, J.M. Calderon Moreno, M. Popa, Quaternary Ti-20Nb-10Zr-5Ta alloy during immersion in simulated physiological solutions: formation of layers, dissolution and biocompatibility, J. Mater. Sci. Mater. Med. 25 (2014) 1099–1114, doi:10.1007/s10856-014-5144-1.